

AD-A187 156

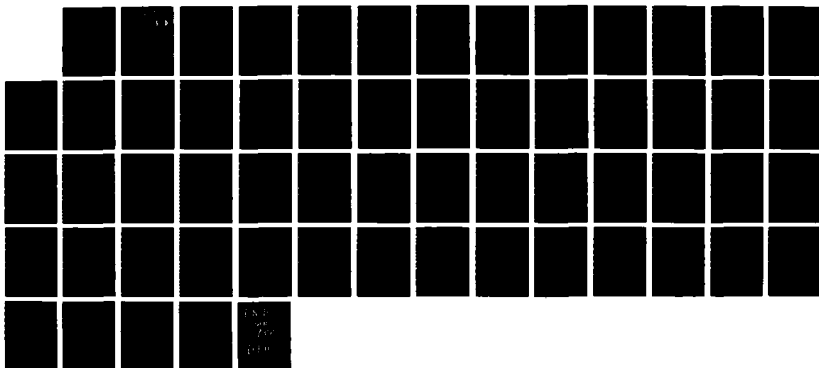
SOLAR PUMPED ALKALI VAPOR LASER(U) PHYSICAL SCIENCES  
INC ANDOVER MA D HAM ET AL. 84 SEP 87 PSI-118/TR-718  
AFOSR-TR-87-1535 F49620-84-C-0118

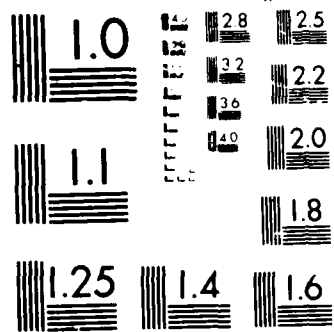
1/1

UNCLASSIFIED

F/G 9/3

ML





AD-A187 156

DTIC FILE COPY

2

~~SECRET~~

PSI-118/TR-718

DTIC  
ELECTE  
NOV 09 1987  
S D

SOLAR PUMPED, ALKALI VAPOR LASER

David Ham  
Mark A. DeFaccio  
Physical Sciences Inc.  
Research Park, P.O. Box 3100  
Andover, MA 01810

AFOSR-TR- 87 - 1535

4 September 1987

Final Report

Distribution Statement

Prepared for  
USAF, AFSC  
Air Force Office of Scientific Research  
Bolling AFB, DC 20332-6448

**DISTRIBUTION STATEMENT A**

Approved for public release  
Distribution Unlimited

Monitoring Organization \_\_\_\_\_

87 / 0 15

23

UNCLASSIFIED

SECURITY CLASSIFICATION OF THIS PAGE

## REPORT DOCUMENTATION PAGE

1a. REPORT SECURITY CLASSIFICATION Unclassified			1b. RESTRICTIVE MARKINGS		
2a. SECURITY CLASSIFICATION AUTHORITY			3. DISTRIBUTION / AVAILABILITY OF REPORT Approved for public release; Distribution Unlimited		
2b. DECLASSIFICATION / DOWNGRADING SCHEDULE					
4. PERFORMING ORGANIZATION REPORT NUMBER(S)  PSI-118/TR-718			5. MONITORING ORGANIZATION REPORT NUMBER(S)  <b>AFOSR-TR- 87-1535</b>		
6a. NAME OF PERFORMING ORGANIZATION  Physical Sciences, Inc		6b. OFFICE SYMBOL (If applicable)		7a. NAME OF MONITORING ORGANIZATION  AFOSR	
6c. ADDRESS (City, State, and ZIP Code) Research Park PO Box 3100 Andover, MA 01810			7b. ADDRESS (City, State, and ZIP Code) Building 410 Bolling AFB DC 20332-6448		
8a. NAME OF FUNDING / SPONSORING ORGANIZATION  Same as 7a		8b. OFFICE SYMBOL (If applicable)  NP		9. PROCUREMENT INSTRUMENT IDENTIFICATION NUMBER  F49620-84-C-0118	
8c. ADDRESS (City, State, and ZIP Code)  Same as 7b			10. SOURCE OF FUNDING NUMBERS		
			PROGRAM ELEMENT NO 61102F	PROJECT NO 2301	TASK NO K1
11. TITLE (Include Security Classification)  "SOLAR PUMPED, ALKALI VAPOR LASER" (U)					
12. PERSONAL AUTHOR(S)  Dr David Ham & Dr Mark A. DeFaccio					
13a. TYPE OF REPORT FINAL		13b. TIME COVERED FROM 1 Sep 84 TO 31 Aug 86		14. DATE OF REPORT (Year, Month, Day) 4 Sep 87	
15. PAGE COUNT 55					
16. SUPPLEMENTARY NOTATION					
17. COSATI CODES			18. SUBJECT TERMS (Continue on reverse if necessary and identify by block number)		
FIELD	GROUP	SUB-GROUP			
			Solar, Laser ←		
19. ABSTRACT (Continue on reverse if necessary and identify by block number) High power lasers based in space have been considered as sources for power transmission, laser propulsion, materials processing and space defense. The feasibility of such systems is based on the cost per unit power delivered, with detailed studies (7,2) indicating that light weight has a greater impact on cost than laser efficiency. Solar radiation is a natural source of power for these devices and two methods for conversion of solar radiation to laser radiation can be considered. An indirectly solar pumped laser would first convert the solar radiation to electricity or longer wavelength blackbody radiation which is then used to power the laser. A directly pumped solar laser would utilize a portion of the solar spectrum to directly pump the laser medium, eliminating the intervening step and substantially reducing the systems weight and complexity. Detailed comparisons (7) showed "a directly pumped laser with an overall efficiency of only 1.5 percent... can compete with an indirectly energized solar laser with an overall efficiency of ten percent". With this in mind, a concept for a directly solar pumped laser was developed based on an alkali vapor (sodium) as the laser medium.					
20. DISTRIBUTION / AVAILABILITY OF ABSTRACT <input checked="" type="checkbox"/> UNCLASSIFIED/UNLIMITED <input checked="" type="checkbox"/> SAME AS RPT <input type="checkbox"/> FOR OFFICIAL USE ONLY			21. ABSTRACT SECURITY CLASSIFICATION Unclassified		
22a. NAME OF RESPONSIBLE INDIVIDUAL Dr Howard R. Schlossberg			22b. TELEPHONE (Include Area Code) 202/767-4906		22c. OFFICE SYMBOL NP

DD FORM 1473, 84 MAR

83 APR edition may be used until exhausted.  
All other editions are obsolete.

SECURITY CLASSIFICATION OF THIS PAGE

UNCLASSIFIED

# CONTENTS

SUBJECT	PAGE
INTRODUCTION	1
CONCEPT	3
ABSORPTION OF SOLAR RADIATION	7
RADIATION TRAPPING	13
LASER GAIN	15
HEAT PIPE OVENS	19
OPTICALLY PUMPED LASERS	37
ROTATIONAL RELAXATION	42
CONCLUDING REMARKS	53



Approved for	
DRIS (CRAC)	<input checked="" type="checkbox"/>
DRIS (AB)	<input type="checkbox"/>
DRIS (C) (D)	<input type="checkbox"/>
Date	
Signature	
Approved by	
Date	
Signature	
A-1	

## INTRODUCTION

High power lasers based in space have been considered as sources for power transmission, laser propulsion, materials processing and space defense. The feasibility of such systems is based on the cost per unit power delivered, with detailed studies(1,2) indicating that light weight has a greater impact on cost than laser efficiency. Solar radiation is a natural source of power for these devices and two methods for conversion of solar radiation to laser radiation can be considered. An indirectly solar pumped laser would first convert the solar radiation to electricity or longer wavelength blackbody radiation which is then used to power the laser. A directly pumped solar laser would utilize a portion of the solar spectrum to directly pump the laser medium, eliminating the intervening step and substantially reducing the systems weight and complexity. Detailed comparisons(1) showed "a directly pumped laser with an overall efficiency of only 1.5%... can compete with an indirectly energized solar laser with an overall efficiency of 10%." With this in mind, a concept for a directly solar pumped laser was developed based on an alkali vapor (sodium) as the laser medium.

The equilibrium components of the sodium vapor are a large percent of atoms and a smaller fraction of diatomic molecules(dimers), the dimers constituting the lasing species. An efficient laser cycle requires that a large fraction of the solar spectrum be absorbed

during the pumping transition, and  $\text{Na}_2$  has a dissociative continuum absorption which peaks at the peak of the solar spectrum. As will be discussed in the sections that follow, the efficiency of a directly pumped laser is proportional to the ratio of the laser wavelength to the average wavelength absorbed. With absorption in the visible and known laser transitions in the infrared the sodium dimer is thus a good candidate for a directly solar pumped laser.

The following sections will present the concept for a directly pumped solar laser, calculate solar absorption efficiencies and estimate the gain of the laser. The experimental program to develop a broadband pumped sodium dimer laser will be reviewed. Because of the high temperature of operation (possibly 900 K), development of a device that allows access for broadband optical pumping while maintaining a vapor of uniform density is a difficult task. Modification of the standard heat pipe oven has been the general direction for the design of two devices, and their performance to date will be discussed.

Another aspect of the experimental program has been the measurement of rate constants for rotation changing collisions between the excited sodium dimer (near the upper laser state) and a second body. I will review the method we used for measuring these rates and present preliminary results for collisions of sodium with Xe, Ar,  $\text{N}_2$ , and He.

## CONCEPT

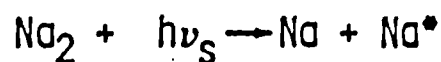
The concept for the proposed solar pumped sodium laser involves several separate processes. Figure 1(3) outlines the overall mechanism for the sodium vapor laser. The lasing medium consists of a sodium vapor, which at 650 degrees celsius has a total vapor pressure of 52.7 Torr with the dimer 11% of the vapor species. Solar radiation is absorbed over a wide wavelength region in the visible via the bound-free absorption by ground state dimers to the dissociative continuum of the B state, resulting in one ground state atom and one atom in the  $^2P_{3/2}$  excited state. The D-line emission from the excited atomic state is strongly trapped because of the high atomic sodium density and large atomic absorption cross section of the D-line. Trapping of the D-line photons pools the solar radiation energy into a relatively narrow wavelength region, necessary for efficient inversion production. This trapped D-line radiation is absorbed via the bound-bound transition from low vibrational levels of the ground state dimer to a narrow band of levels in the  $A'\Sigma_u^+$  state of the dimer, this being our upper laser level. The absorption of the D-line occurs on the inner turning point of the A state potential, with the laser transition occurring on the outer turning point of this excited level resulting in a ground state dimer of high vibrational level. This lower laser level relaxes to its thermal population through collisions with any species, thus maintaining the inversion.

## SOLAR PUMPED SODIUM LASER

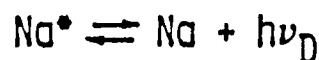
### Composition



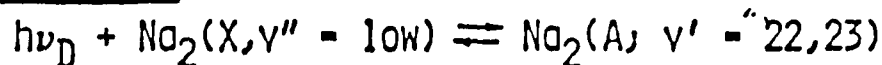
### Absorption



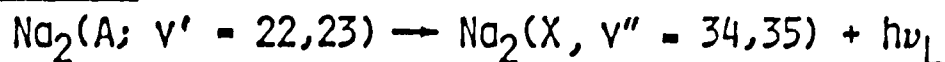
### Radiation Trapping



### Upper Level Excitation



### Stimulation Emission



### Lower Level Relaxation

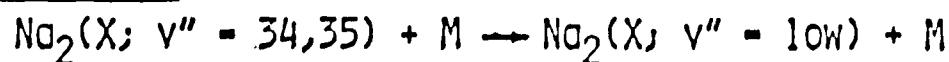


FIGURE 1 Proposed mechanisms for a broadband pumped sodium dimer laser.

Figure 2(3) shows the potential energy versus internuclear separation exhibiting the molecular and atomic states involved, with the relevant transitions indicated with arrows. The two arrows connected by an arc in the ground state constitute the locus of vibrational levels with enough energy to photodissociate via classically allowed Franck-Condon transitions at the corresponding internuclear separation. From this curve we see that the average energy of this transition is around 20,000 wavenumbers, while the solar spectrum peaks at around 20,500 wavenumbers, providing a good overlap of the solar spectrum with the the solar absorption transitions. The far right arrow indicates the deexcitation of the  $^2P_{3/2}$  state of the atom by D-line emission. The two arrows connecting the ground state dimer with the A-state correspond to absorption of the D-line photon by the ground state to the inner turning point of a level in the A-state, with the laser transition occurring at the outer turning point of this level.

Details of the mechanisms just introduced will be covered in the following sections with calculations of the solar absorption efficiencies, trapped radiation lifetimes and laser gain.

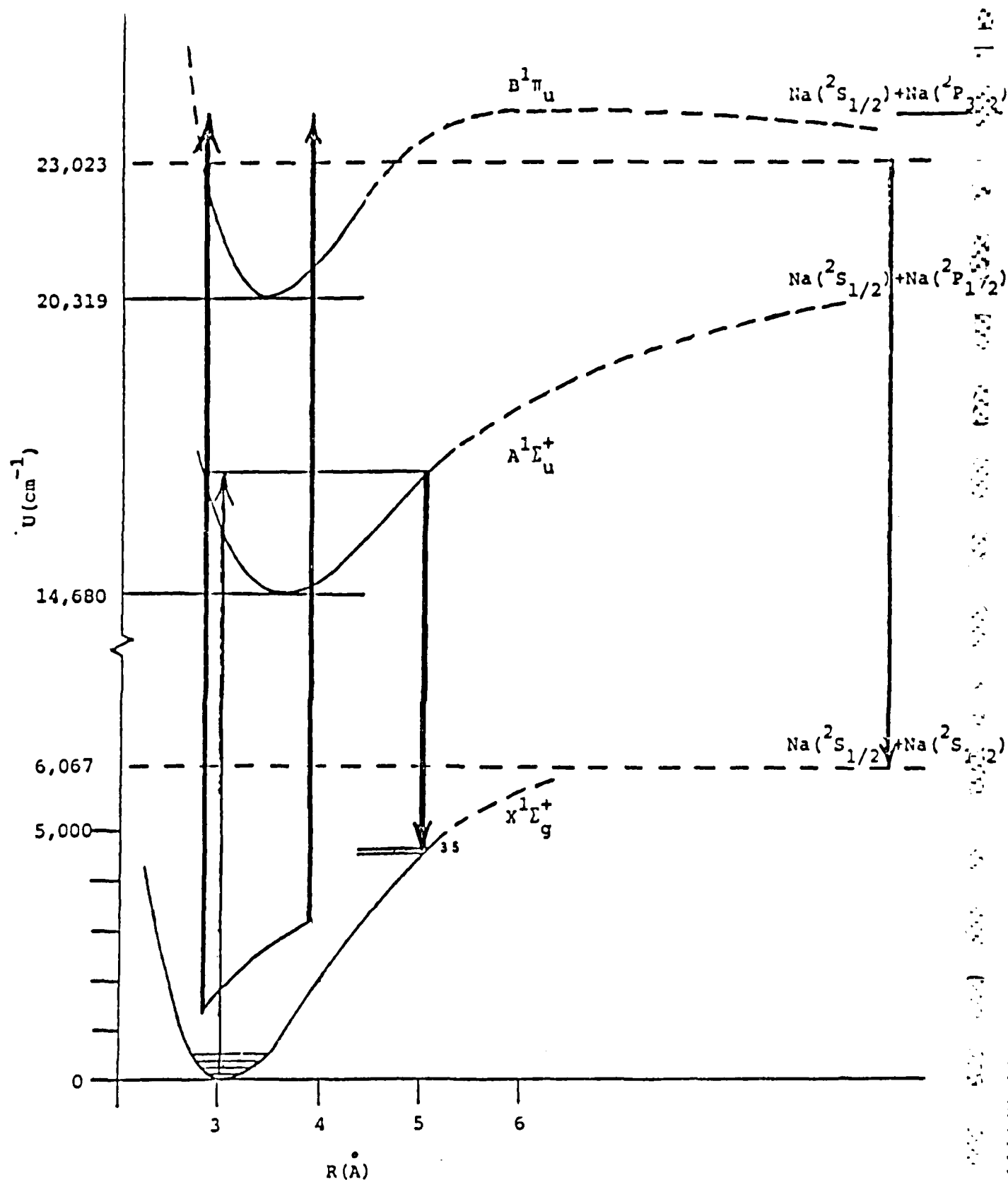


FIGURE 2 Potential energy versus internuclear separation diagram of  $\text{Na}_2$ , with arrows indicating relevant transitions of the sodium dimer laser.

## ABSORPTION OF SOLAR RADIATION

Most of the absorption of the solar radiation will occur via the bound-free transition  $X\Sigma_g^+ \rightarrow B'\Pi_u$  diagrammed in figure 2. The photodissociation continuum of  $Na_2$  has been measured (3) using laser-induced fluorescence of the atomic D-lines under conditions where collisional processes were absent. The D-line emission as a function of exciting laser wavelength is shown in figure 3, and agrees within experimental errors with the results of Callender et al. (5,6) and Kraulinia and Yanson (7). This curve of D-line intensity is determined mainly by the Boltzmann distribution among the vibrational levels from which photodissociation can take place at the given laser frequency. The measurements of Ref. (3) confirmed that the atomic fluorescence resulted from direct excitation to the dissociative continuum of the diatomic parent, and that collisional energy transfer from excited molecules and collision-induced predissociation of the excited molecules do not contribute significantly to the  $3^2P_{3/2}$  atomic population.

The calculation of the fraction of the solar radiation absorbed by this dissociative continuum requires a value for the cross section associated with these transitions. The data of reference (7) will be used, and are plotted in figure 4. These data were taken at 500 degrees Kelvin, while the temperatures of interest are around 925 degrees Kelvin.

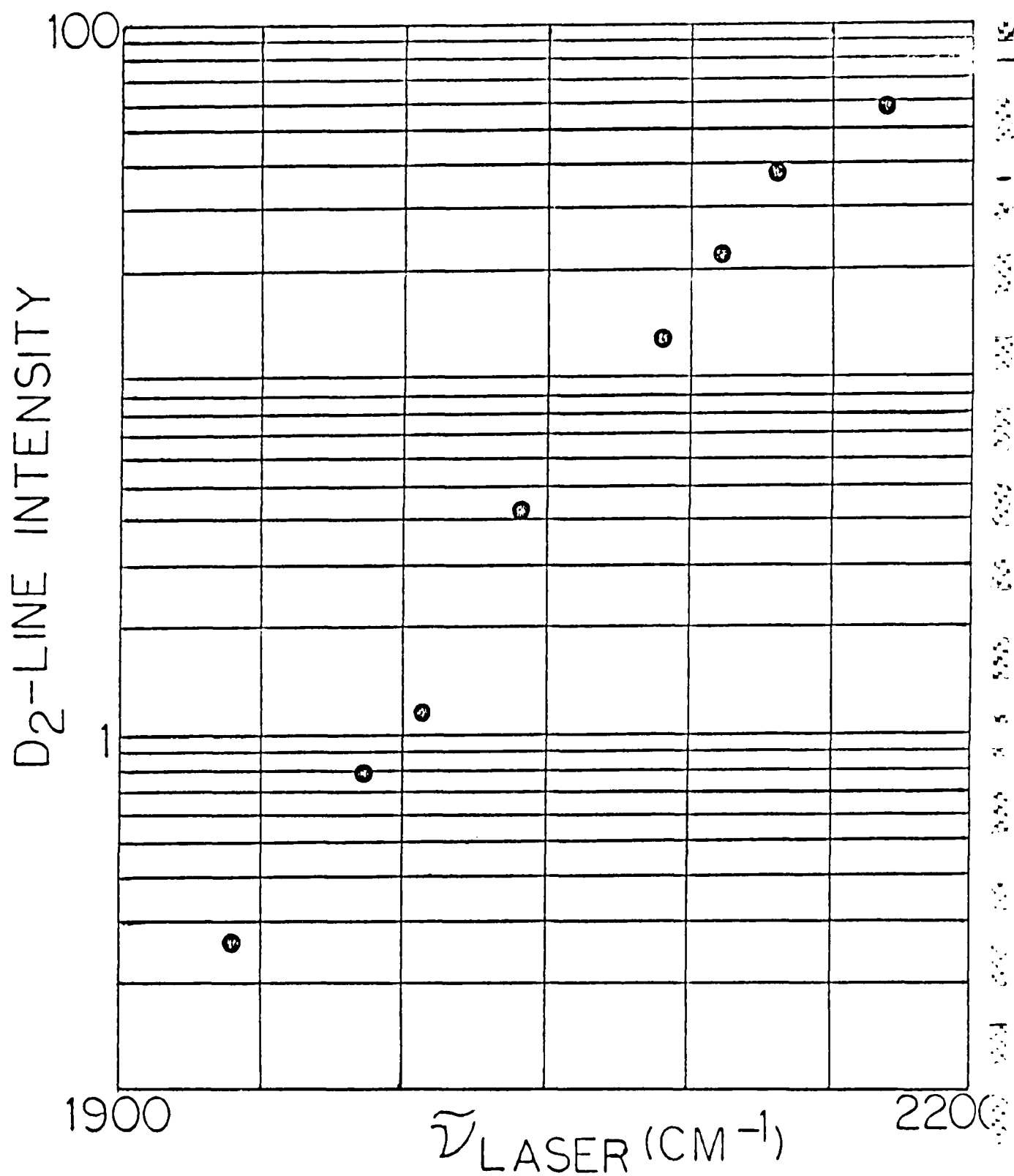


FIGURE 3 D<sub>2</sub>-line atomic fluorescence intensities from laser dissociation of Na<sub>2</sub>, as a function of laser wavelength. Data from Ref. (3).

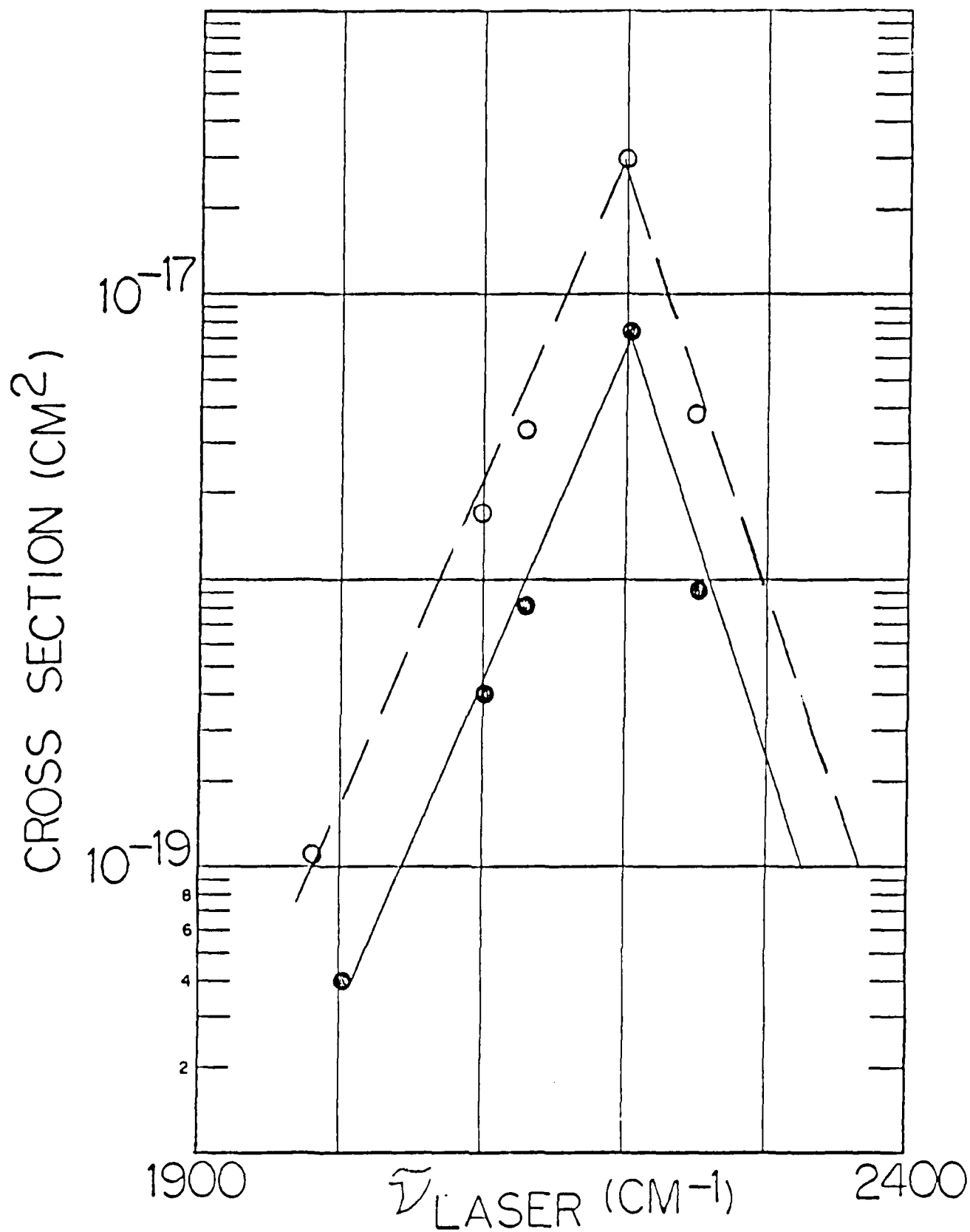


FIGURE 4 Cross section for the reaction  
 $\text{Na}_2(X^1\Sigma_g^+)+h\nu\rightarrow\text{Na}(^2S_{1/2})+\text{Na}(^2P_{3/2})$ .  
 Solid line data from Ref. (7) at 500 K.  
 Dashed line extrapolated to 925 K.

Because the cross section was shown to increase with temperature we extrapolated to higher temperatures by multiplying the cross section at 500 degrees Kelvin by the population ratio of the ground state dimer in the  $v''=10$  vibrational level at 925 and 500 degrees Kelvin. This is the lowest level contributing to the transitions, those levels above  $v''=10$  will increase at a faster rate than the  $v''=10$  level and thus this calculation provides a conservative estimate for the cross section at 925 K. A plot of this extrapolated cross section is also shown in figure 4.

The procedure followed to determine the percentage of solar radiation absorbed, was to calculate the cross section at which the solar irradiance defined in 1.) below, dropped to  $1/e$  of its incident value.

$$1.) \quad I(X) = I(0) \exp(-\sigma [Na_2] \cdot X)$$

with  $\sigma$  = cross section

$[Na_2]$  = sodium density

$X$  = linear distance into vapor

The frequency dependent cross section of figure 4 was then used to determine the bandwidth over which the cross section satisfies the relation,

$$2.) \quad \sigma > 1/([Na_2] \cdot X),$$

corresponding to the intensity dropping by  $1/e$ . The bandwidth determined in this manner is taken as the region of essentially total absorption of the incident solar radiation.

Data from reference (8) on the solar irradiance outside the earth's atmosphere was used to determine what percentage of the incident solar irradiance lies within the bandwidth determined above, for a given path length of sodium vapor. Figure 5 is a plot of the percent of solar radiation absorbed versus temperature for two different path lengths in which the optical depth exceeds unity, as determined by 2.) above. Evidently this bound-free absorption can be large, with figure 5 a conservative estimate of only the major anticipated absorption mechanism.

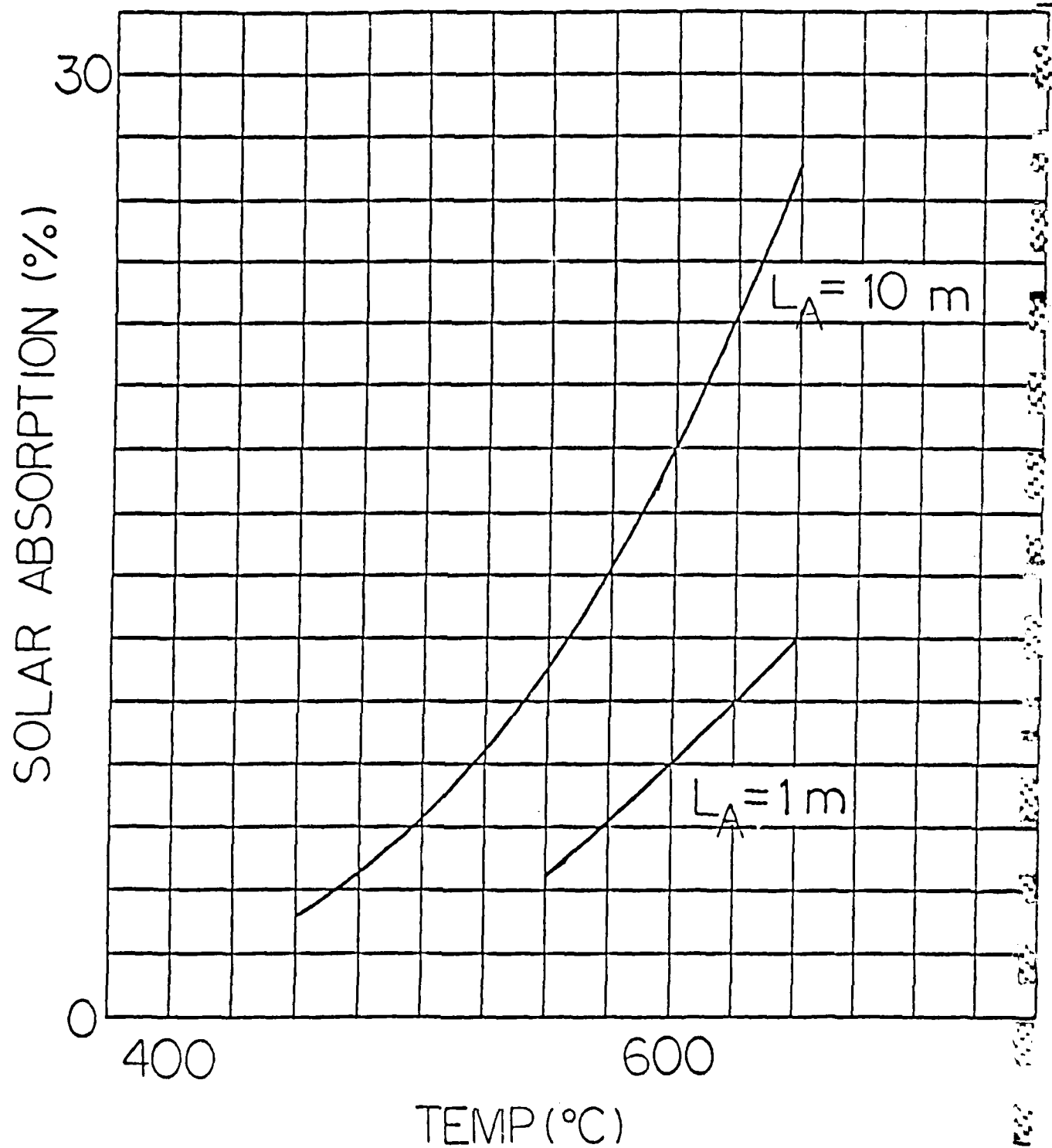


FIGURE 5 Calculated absorption of solar irradiance outside the earth's atmosphere by the dissociative continuum of  $\text{Na}_2$ .  $L_A$  is the absorption depth.

## RADIATION TRAPPING

Radiation trapping refers to the increased decay time of a pulse of resonance radiation transmitted through a dense vapor. A trapped photon will undergo many absorptions and re-emissions by the resonant species before escaping, resulting in an effective lifetime for the photon many times larger than the spontaneous radiative lifetime. The cross-section for this resonant absorption of Na D-line is larger than  $10^{-13} \text{ cm}^2$  (3), trapping the D-line for times an order of magnitude longer than the spontaneous lifetime. Reference (3) compared trapped lifetimes for the Na D-line as measured by several groups(9-11) to the theories of both Holstein(12) and Milne(13). Figure 6 is a plot of the effective lifetime as a function of Na density showing the more than ten-fold increase in the lifetime of the resonant D-line. Extrapolation of the increase in the lifetime to Na densities of interest ( $10^{17} \text{ cm}^{-3}$ ) is beyond the scope of the available data, though a discussion of probable limits for the effective lifetime by Ref. (3) concluded that lifetimes of several microseconds were reasonable.

The uniform dissociative absorption of solar radiation discussed in the last section will thus pool solar energy into the trapped atomic D-line. This pooling and establishment of a high energy density within a relatively narrow bandwidth is essential to success of this laser concept. The trapped radiation pumps the upper laser level as discussed in the next section.

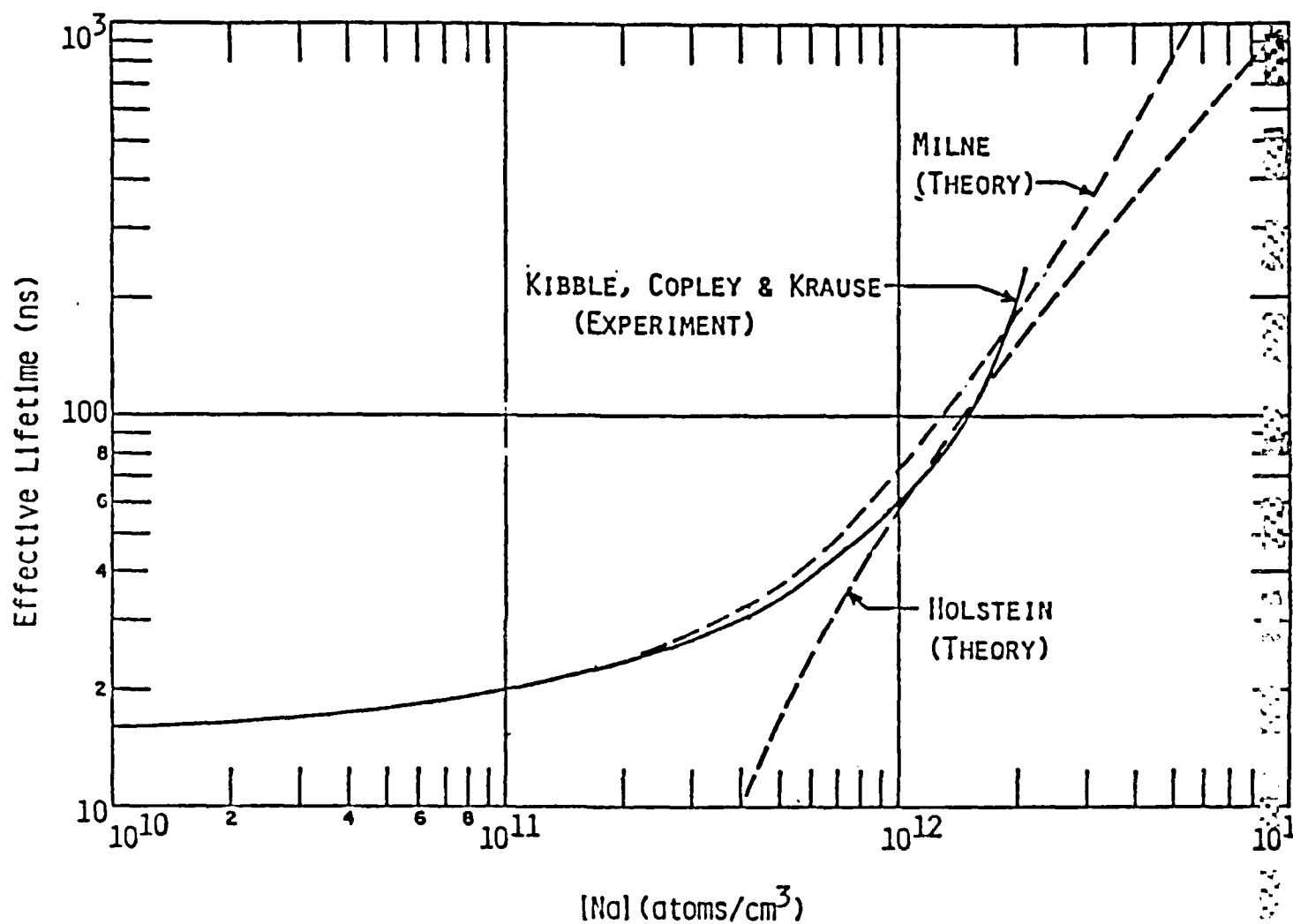
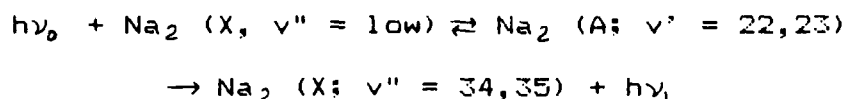


FIGURE 6 Comparison of measured values for the Na density dependence of the effective lifetime of the trapped Na D-line with two theories.

## LASER GAIN

The upper laser level will be optically excited by the trapped Na D-line resonance radiation, producing a relatively narrow range of vibrational-rotational states:



Sodium dimer A state lasers have been made with optical pumping by lasers near the resonant D-line(14-16), and hundreds of laser lines have been observed by the author with dye laser pumping in the red. It is expected that laser action can be achieved by D-line excitation if a high enough density of radiation can be produced within the vapor.

Emission from the  $A'\Sigma_u^+$  of  $\text{Na}_2$ , excited by trapped D-line radiation was measured by Ham(17), the observed spectrum shown in figure 7. Uniform excitation of sodium atoms was accomplished by chemiluminescence from the reaction of sodium atoms with a number of halogens. The author has measured the fluorescence in the region from about 7800 to 8200 Å from sodium vapor excited by a dye laser tuned to the atomic D-line. This spectrum is shown in figure 8 and exhibits the same structure as figure 7 in the region measured. The measurements of Ref. (17) on the relative intensities in the spectrum of figure 7 indicate that at 300 degrees Celsius about 30% of the  $\text{Na}(3^2P)$  excitation energies escapes via spontaneous emission from  $\text{Na}_2(A)$  with fluorescence as shown in figures 7 and 8. At the higher temperatures and densities

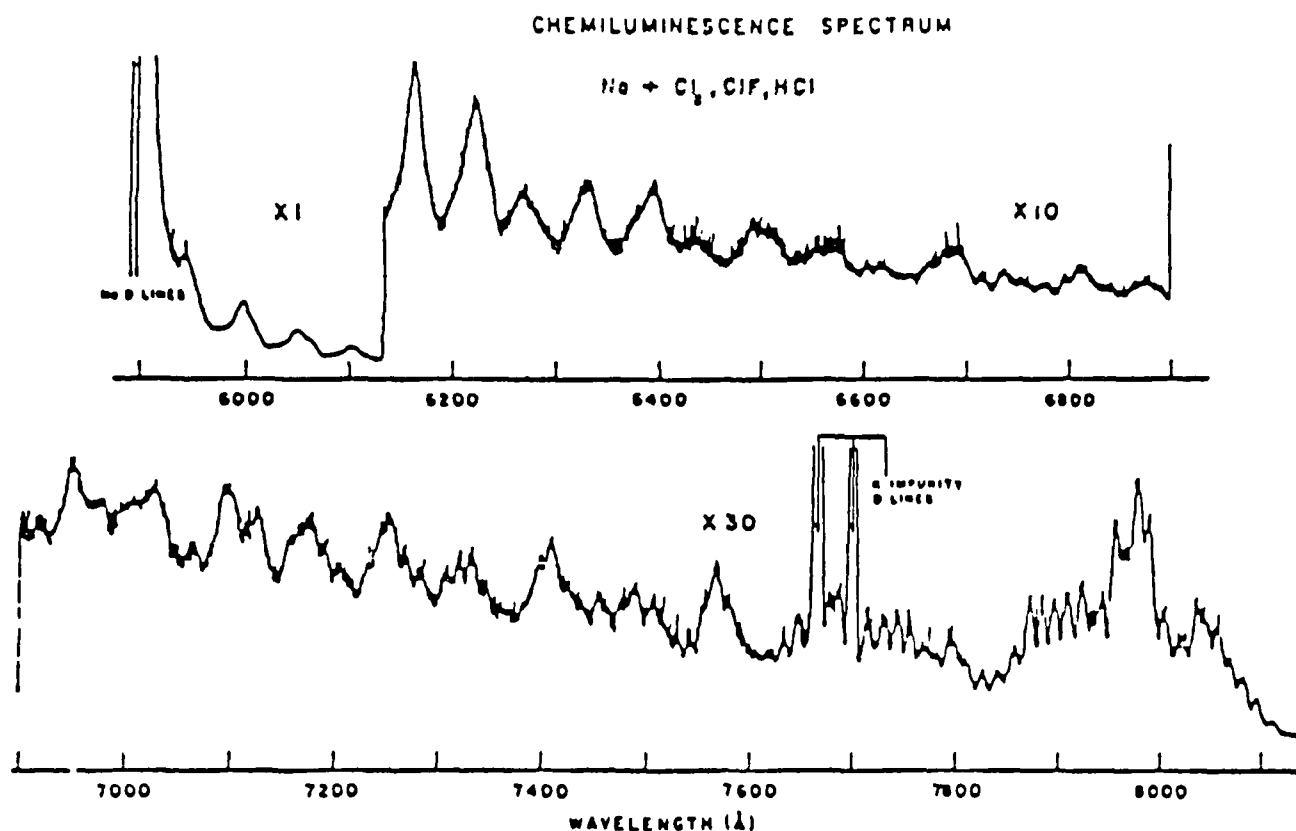


FIGURE 7 Emission from  $\text{Na}_2(\text{A}^1\Sigma_u^+)$  excited by chemiluminescent emissions from sodium atoms.

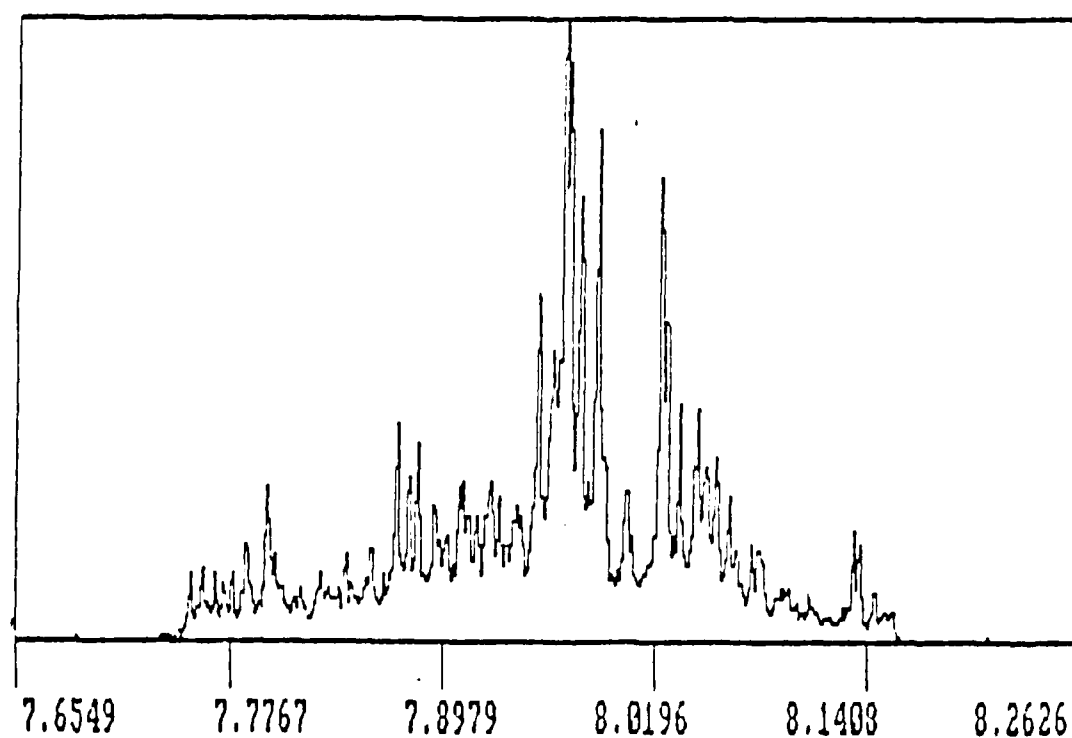


FIGURE 8 Emission from  $\text{Na}_2(\text{A}^1\Sigma_u^+)$  excited by a dye laser tuned to the sodium atomic D-line.

under consideration this percentage will increase because of the large trapping time for the D-line radiation. Because this emission is to high lying levels of the ground state, whose thermal populations are less than  $2 \times 10^{-4}$  of the total  $\text{Na}_2$  populations, a population inversion is likely.

An estimate of the expected gain for this sodium vapor laser excited by a broadband source can be made using a gain equation derived by Rather (1) for the direct solar pumping of lasers. Equation 27 from Ref. (1) for the product of the laser gain times the absorption depth  $L_A$  is :

$$GL_A = \frac{0.061}{[\exp(2.44/\lambda_p) - 1]} \frac{1}{(f/\#)} \left\{ \frac{\lambda_L}{\lambda_p} \right\} \left\{ \frac{\Delta\lambda_p}{\Delta\lambda_L} \right\} \left\{ \frac{\tau_{loss}}{\tau_{rad}} \right\}$$

where p refers to pump and L to laser, all wavelengths in microns. The  $f/\#$  is the f-number of the optical system which reflects the solar radiation into the laser medium, a reasonable value for the  $f/\#$  being .7. The ratio of the mean time for upper laser level depopulation to the spontaneous emission time ( $\tau_{loss} / \tau_{rad}$ ), can be estimated as unity, since even rapid collisional relaxation will not compete with the spontaneous emission and

$$1/\tau_{loss} = 1/\tau_{rad} + 1/\tau_{coll}$$

where  $\tau_{coll}$  refers to the 1/e time for collisional relaxation.

Using ( $\lambda_{p, \text{max}}$  as  $.45 \mu\text{m}$ ,  $\lambda_L = .8 \mu\text{m}$ , a pump bandwidth  $\Delta\lambda_p$  from figure 4 of  $4500 \text{ cm}^{-1}$ , and a laser bandwidth of  $.05 \text{ cm}^{-1}$  gives me a large

value of around 400 for  $GL_A$  (where the absorption depth  $L_A$  is taken as 100 cm), consistent with the high gains of  $> 4 \text{ cm}^{-1}$  reported in Ref. (14). Thresholds of  $1/\mu_j$  for pulsed laser pumping of  $\text{Na}_2(\text{A-X})$  were measured (14), though we expect that pumping with incoherent broadband sources will have somewhat higher thresholds. Still, these low thresholds combined with the high calculated gain indicate that pulsed operation of the sodium dimer laser described should be achievable. CW operation may be limited by collisional relaxation of the lower laser level, which is necessary for maintaining a population inversion. The successful CW operation of the more extensively studied  $\text{Na}_2(\text{B-X})$  system indicates that the inversion will most likely be maintained, and broadband optical pumping of the  $\text{Na}_2(\text{A-X})$  system can be operated in the CW mode.

## HEAT PIPE OVENS

Originally designed as devices for very high thermal conductance, heat pipe ovens are used extensively as spectroscopic tools for the study of vapors. The operation of a heat pipe(18) is based on a well known method for the transfer of large amounts of heat with a small temperature difference. This is accomplished by the evaporation of a liquid, transport of the vapor to a cooler region and condensation of the vapor. Continuous operation requires that the condensed liquid return to the evaporation region. In a heat pipe this is accomplished by using the effect of surface tension. The operation of a heat pipe is diagrammed in figure 9. The heat pipe consists of a closed tubeing with a capillary structure, or wick on its inner walls. The wick is saturated with a wetting liquid and the evaporator maintained at a higher temperature than the condenser by heating. This temperature difference produces a pressure gradient which drives the vapor to the condenser. The depletion of liquid by evaporation drives the liquid-vapor interface into the wick, the adjacent liquid pressure being  $P_E - \gamma/R_E$ ,  $R_E$  the liquid-vapor interface local radius of curvature(meniscus) and  $\gamma$  the surface tension. In the condenser region the liquid pressure is  $P_C - \gamma/R_C$ , with  $R_C$  often limited by the heat pipe structure. The resulting pressure available to drive liquid from condenser to evaporator

$$P_{TOT} = P_C - P_E + 2\gamma/R_E - 2\gamma/R_C ,$$

can be made positive by choosing a wick of the appropriate pore size.

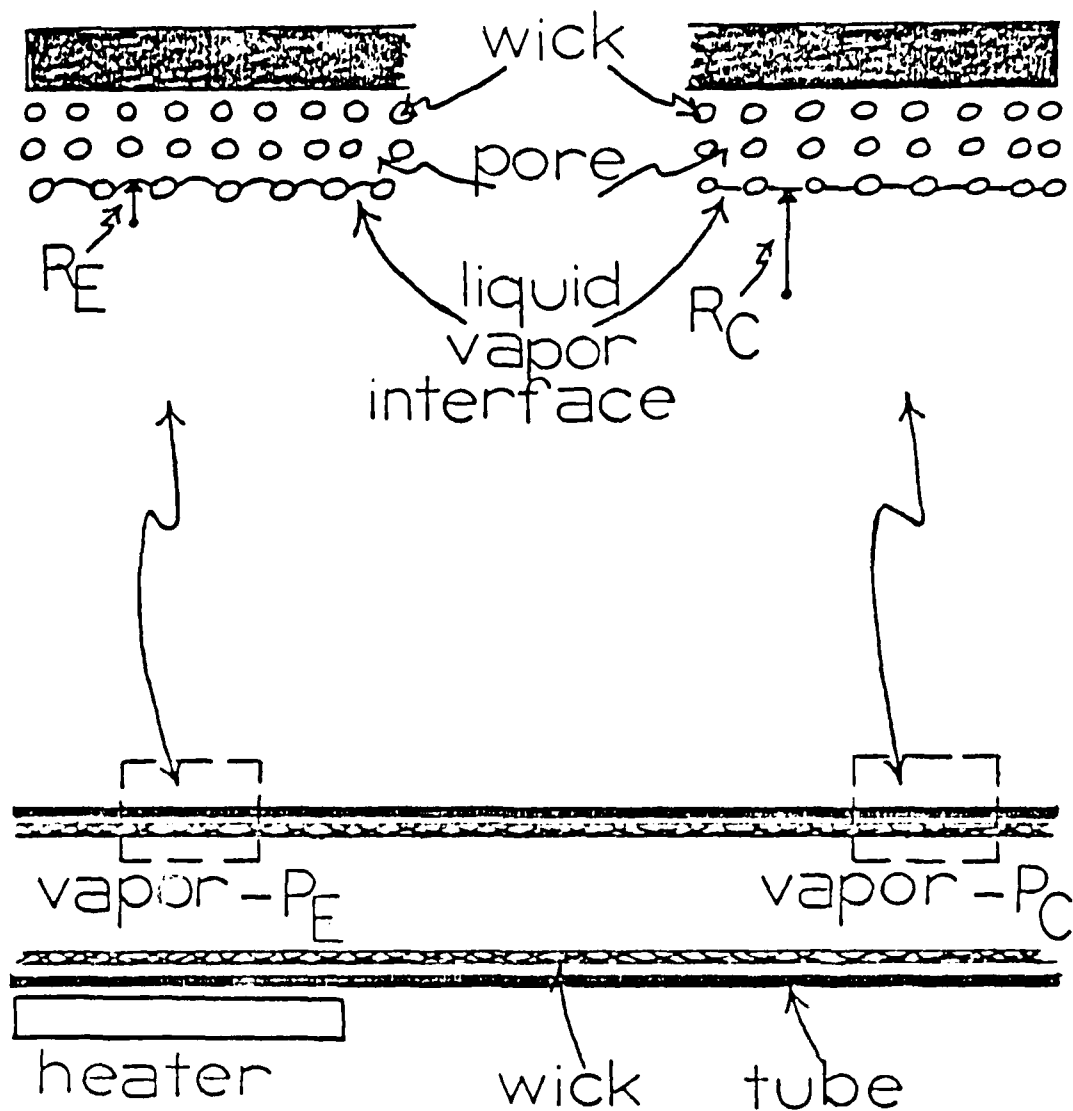


FIGURE 9 Schematic diagram of the operation of an ideal heat pipe.  $R_E$  is the liquid-vapor interface meniscus in the evaporator region,  $R_C$  in the condenser region.  $P_E$  and  $P_C$  are the vapor pressures in the two regions. Liquid flows from the condenser to the evaporator if

$$P_C - P_E + 2\sigma/R_E - 2\sigma/R_C > 0$$

The use of a heat pipe for spectroscopic purposes requires that the device have windows. C. R. Vidal and J. Cooper (19), utilizing a method similiar to Bohdansky and Schins, introduced the standard method for producing well defined metal vapors in the heat pipe oven. Diagrammed in figure 10 is a simple schematic of a heat pipe oven and its operation. It consists of a central region designed like a heat pipe, a tube with a wick on its inner walls. Typically the wick consists simply of a woven mesh, stainless steel is used by the author for the sodium heat pipes. The mesh size does not appear to be critical, with a variety of mesh sizes working well in various devices. The central region is used as the evaporator, a cylindrical heating element enclosing the tube to provide uniform heating. There are thus two condenser regions, at both ends of the tube, where cooling coils are wrapped around the tube to provide a well defined boundary layer between the evaporator and condenser. The ends of the tubes have windows mounted with the appropriate O-ring structure to provide a vacuum seal. Gas/vacuum inlets are placed near the windows in both condenser regions, providing access for pumping the device down to low pressure levels and for leakage of small amounts of an inert gas into the oven.

Operation of the heat pipe oven begins by filling the oven to a known pressure with an inert gas, such as Argon. With the evaporator region loaded with a sample of metal (sodium), we then begin heating in this region. The sodium melts and starts

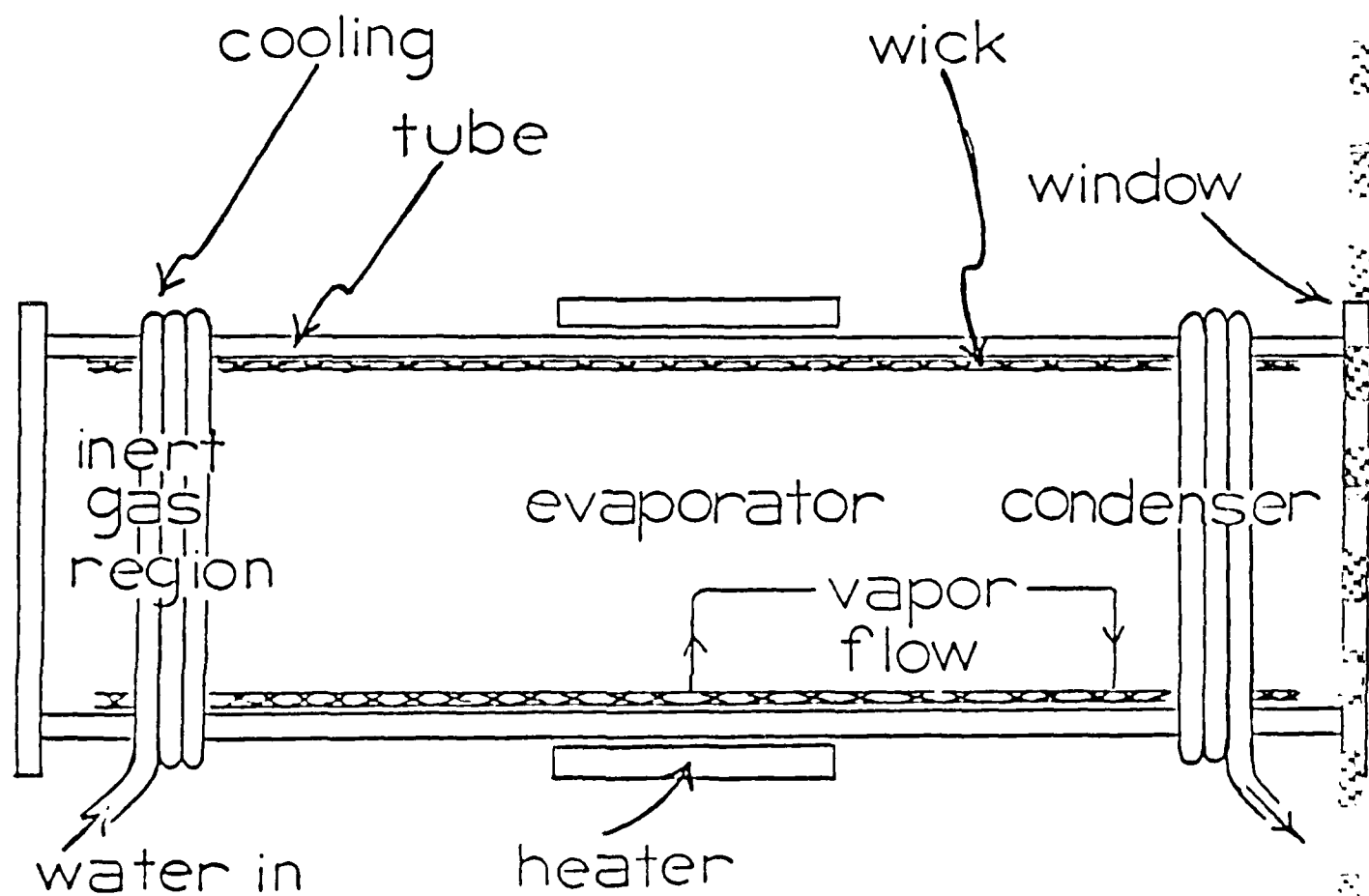


FIGURE 10 Schematic diagram of the operation of a heat pipe oven used for spectroscopic measurements.

wetting the wick. The sodium begins evaporating at the temperature given by the vapor pressure curve of the metal for which the sodium vapor pressure approximately equals the pressure of the inert gas. The evaporating sodium then flows to both ends of the tube where it condenses onto the wick and flows back to the evaporator. When it reaches a steady state the central portion is filled with the sodium vapor at a pressure determined by the pressure of the confining inert gas, which, because of the pumping action of the sodium vapor, is swept out of the central region and into the ends. Mixing of the two gases does occur in a short boundary layer between the evaporator and condenser, with a thickness much less than the length of the vapor zone. Because the inert gas remains in the cooler ends of the oven, it protects the windows from deposition of the metal vapor which would otherwise cloud the windows quickly. The temperature of operation is determined mainly by the inert gas pressure which can be varied, and the power input to the heaters which is also adjustable. Therefore, a range of temperatures, and thus vapor densities, is available to the user of a heat pipe oven.

The heat pipe oven has a number of characteristics which make it an extremely useful device for the study of metal vapors, and in our case sodium. Because evaporation and condensation take place at essentially the same temperature, the zone over which the vapor flows from the evaporator to the condenser is isothermal. The pressure gradient which creates the flow need not be very large, and typically

the temperature changes by only about 1-2 degrees celsius over the vapor zone. Only in the boundary layer zone between the metal vapor and inert gas does the temperature drop off rapidly as the vapor condenses. A simple thermocouple can be used to determine the temperature within the zone to 1 degree Celsius accuracy, and a simple manometer will easily determine the pressure with 1% accuracy. The evaporation and condensation cycles the metal goes through purifies it so that after a certain period of operation a very pure zone of the metal vapor exists. Most of the impurities will be swept out into the cooler region where they will condense or remain in the gaseous phase. By starting with an impurity concentration that is small, any impurities that have a higher vapor pressure than the metal will not be saturated and will not be in equilibrium with their liquid phase. Thus they will not condense again and the pumping action of the metal sweeps them out to the colder regions. Impurities with a vapor pressure much lower than the metal will have no effect on spectroscopic measurements, while those with vapor pressures comparable to the metal will again not be saturated.

Figure 11(20) is a plot of the temperature of sodium in a heat pipe versus axial position for two different powers. Note that as one changes the power it is the length of the metal vapor zone which undergoes the largest change. The small increase in temperature is due to the increase in the buffer gas pressure as its volume decreases, since the temperature is determined by the buffer gas

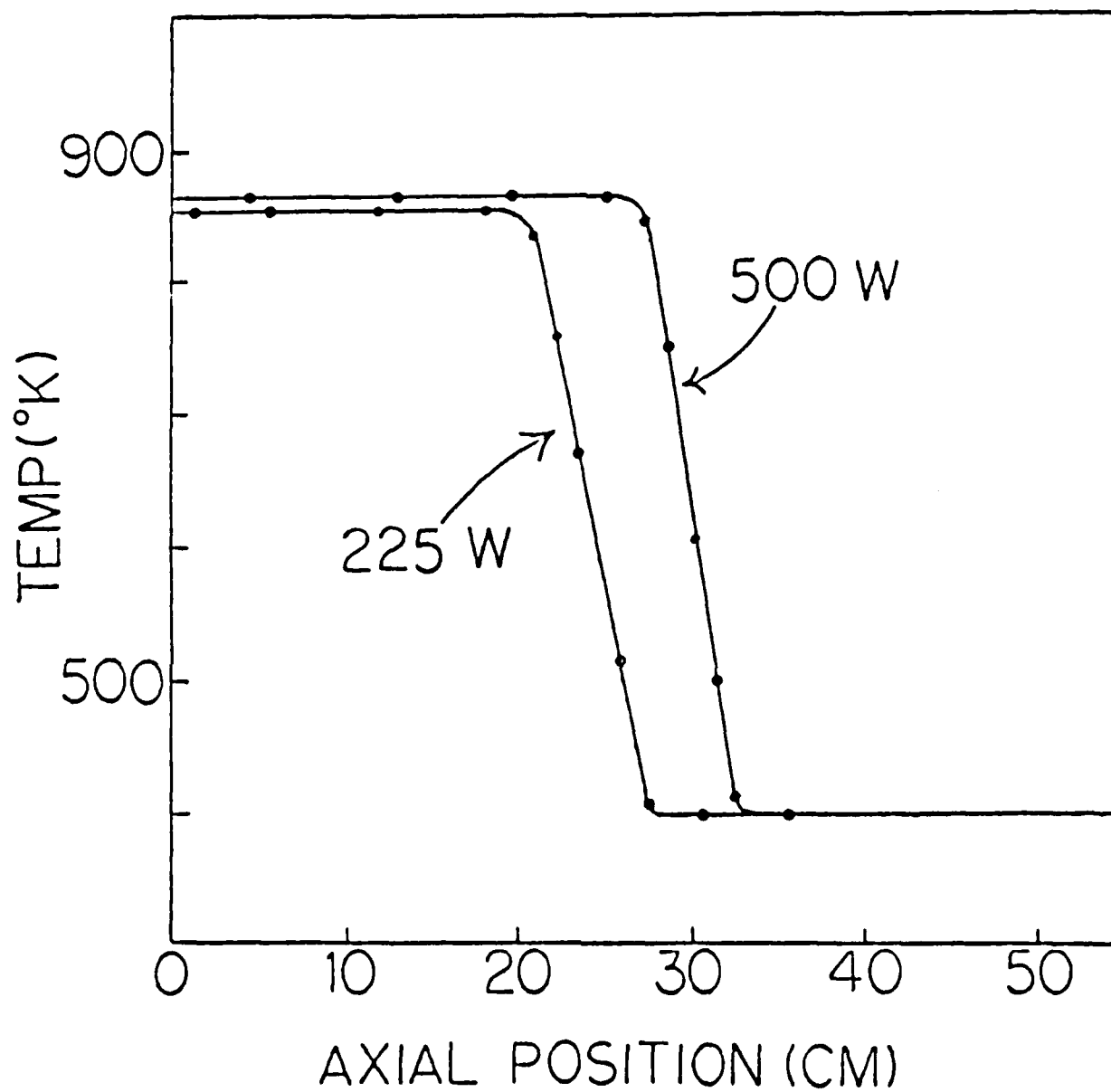


FIGURE 11 Axial temperature variation along the vapor-liquid interface of a sodium-argon heat pipe.

pressure and the metals vapor pressure curve.

It is the well defined and uniform vapor density that make the heat pipe oven such an attractive device for the production of a lasing medium such as sodium vapor. The difficulty in using it for our concept is modifying it to allow access for broadband optical pumping, without eliminating its positive qualities that are very geometry dependent. An ideal heat pipe oven is long with an inside radius much less than its length, and will provide a very uniform vapor over a long path length. To date, we have studied three devices, one a standard crossed heat pipe oven borrowed from Stwalley et. al. at the University of Iowa Laser Facility, a rectangular heat trough designed at the beginning of the program, and a new device designed more in line with the standard heat pipe.

Figure 12 is a diagram of the three devices just mentioned, the crossed heat pipe on top, the rectangular heat trough in the center and the latest device on the bottom. The crossed heat pipe oven is a variation on the original heat pipe oven device which allows access for observation from five directions. For example, in a laser induced fluorescence studies, one axis can be used for propagation of the exciting laser, another axis for the use of a probing laser and the last port for detecting devices. Its operation is similar to the standard heat pipe oven with

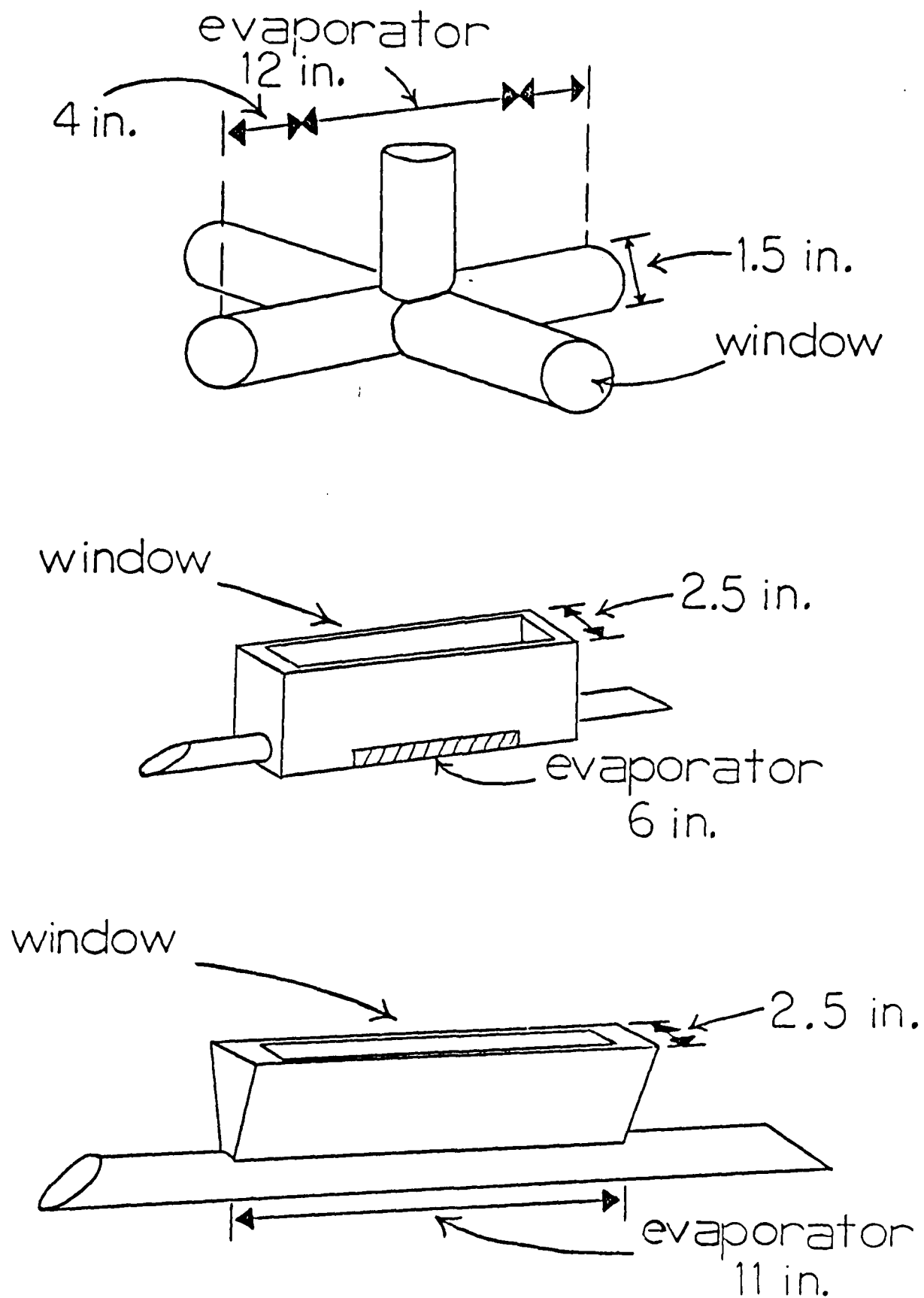
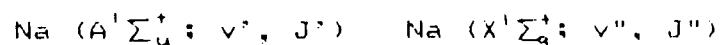


FIGURE 12 The three heat pipe oven devices used in the experimental program. The top one is a standard, crossed heat pipe oven, middle is a rectangular heat trough with open top and the bottom one is the latest device with open top.

the extra ports a perturbation on the standard design. This crossed heat pipe oven was used to produce a temperature calibration curve for determining the temperature profile in the other devices, and for measurement of rotational relaxation rates of the dimer by collision with a second body. The remainder of this section will discuss the operation of the other devices and the methods used for their characterization.

Our approach for measuring local temperatures in the heat pipe oven devices is to measure fluorescence ratios excited from different ground state vibrational levels. The fluorescence intensities are determined by the temperature dependent Boltzmann ratios. An invaluable tool used in this experimental program is an optical multichannel analyzer, consisting of Reticon diode array with imager intensifier interfaced to an IBM AT personal computer, coupled to a Jarrell-Ash quarter meter Spectrometer. I will refer to this device, diagrammed in figure 13, as the OMA. The grating used most extensively in the spectrometer had 1200 lines per millimeter, blazed at 5200 Å, and provided 4 Å resolution over a bandwidth of about 400 Å. An example of a Helium-Neon laser induced fluorescence spectrum obtained in the crossed heat pipe oven is shown in figure 14. Assignment of the lines in this spectrum was made by K. K. Verma et. al. (21), including the ground state dimer levels pumped by the He-Ne laser and the relative intensities of the induced fluorescence for the transitions



The ground state vibrational levels that are pumped by the He-Ne are,

$$v'' = 2, 4, 6, 8.$$

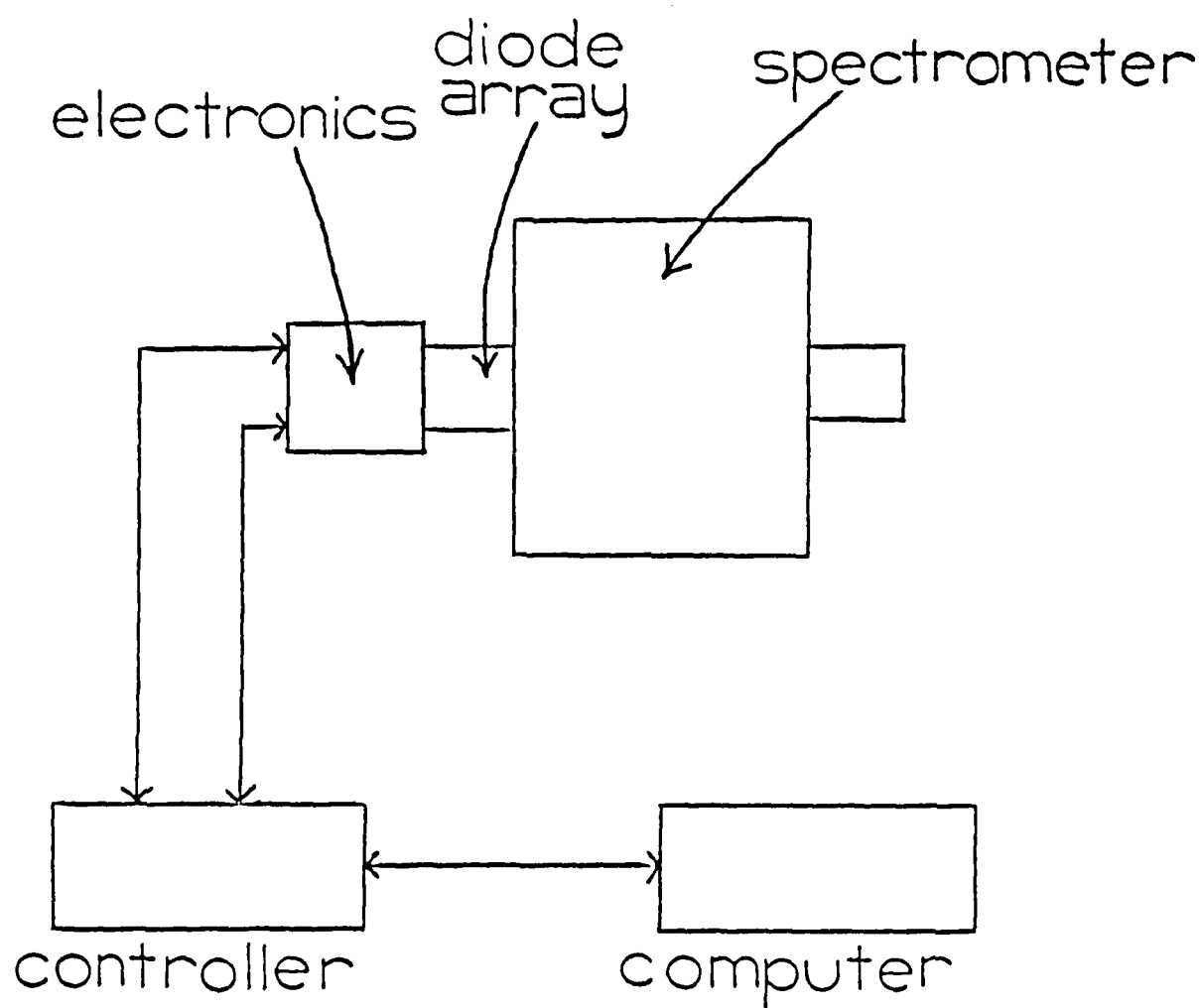


FIGURE 13 Block diagram of the Optical Multi-channel Analyzer, consisting of Jarrell-Ash spectrometer, a Reticon diode array and associated electronics interfaced to an IBM AT computer.

Fluorescence  
pumped from  $\text{Na}_2(X, v'')$

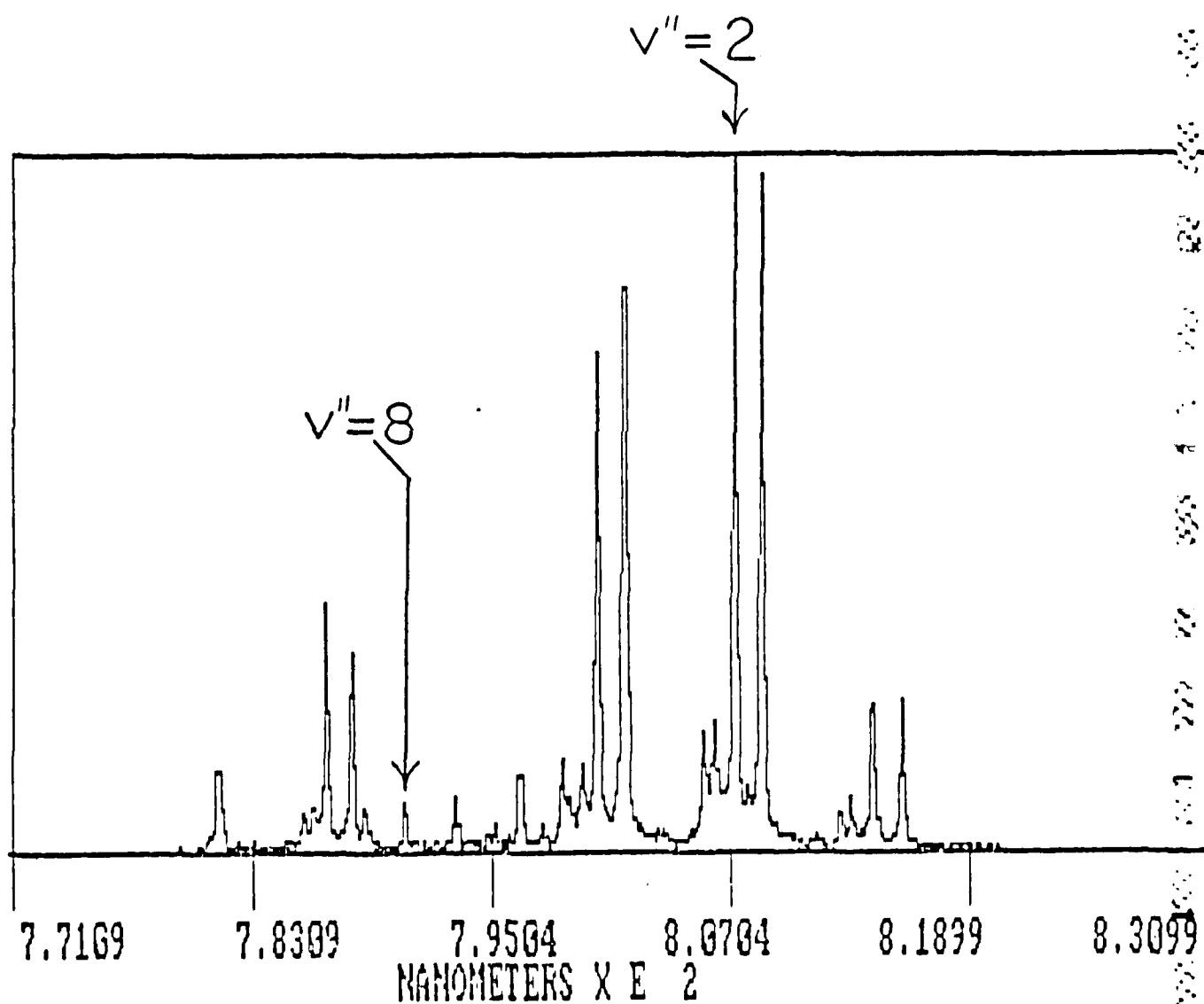


FIGURE 14 He-Ne laser induced fluorescence spectrum of  $\text{Na}_2(A'\Sigma_u^+)$  obtained with the OMA.

Of interest for an accurate temperature measurement is the fluorescence due to pumping from the ground state dimer with vibrational levels of  $v''=2$  and  $v''=8$ . The intensity of the individual lines in the LIF (laser induced fluorescence) spectrum are directly proportional to the Boltzman distribution of the vibrational levels of the ground state dimer, which is a temperature dependent function. The ratio of LIF intensities pumped from different ground state vibrational levels will thus be a function of temperature and can be utilized to measure temperature. The  $v''=2$  and  $v''=8$  levels provide the most accurate temperature measurement, since their population ratio is the most temperature dependent. The two peaks utilized to produce a calibration curve are noted in figure 14. The experimental arrangement used to acquire our calibration is shown in figure 15. The crossed heat pipe was used for this purpose, with a chromel-alumel thermocouple utilized to determine the temperature within a few degrees Celsius at the object position of the DMA. By varying the buffer gas pressure and heater power a range of temperatures from about 300 degrees celsius to 550 degrees celsius were achieved, with spectrum similar to that of figure 14 taken at each temperature. The resulting plot of LIF intensity ratios for the two lines shown in figure 14, versus the inverse temperature is shown in figure 16. The scatter of the data points is due to the large difference in relative intensities of the two lines originating from  $v''=2$  and  $v''=8$ . A pair of LIF lines pumped from the same levels, but of more comparable intensity have been identified in another part of the spectrum and should provide a more accurate calibration.

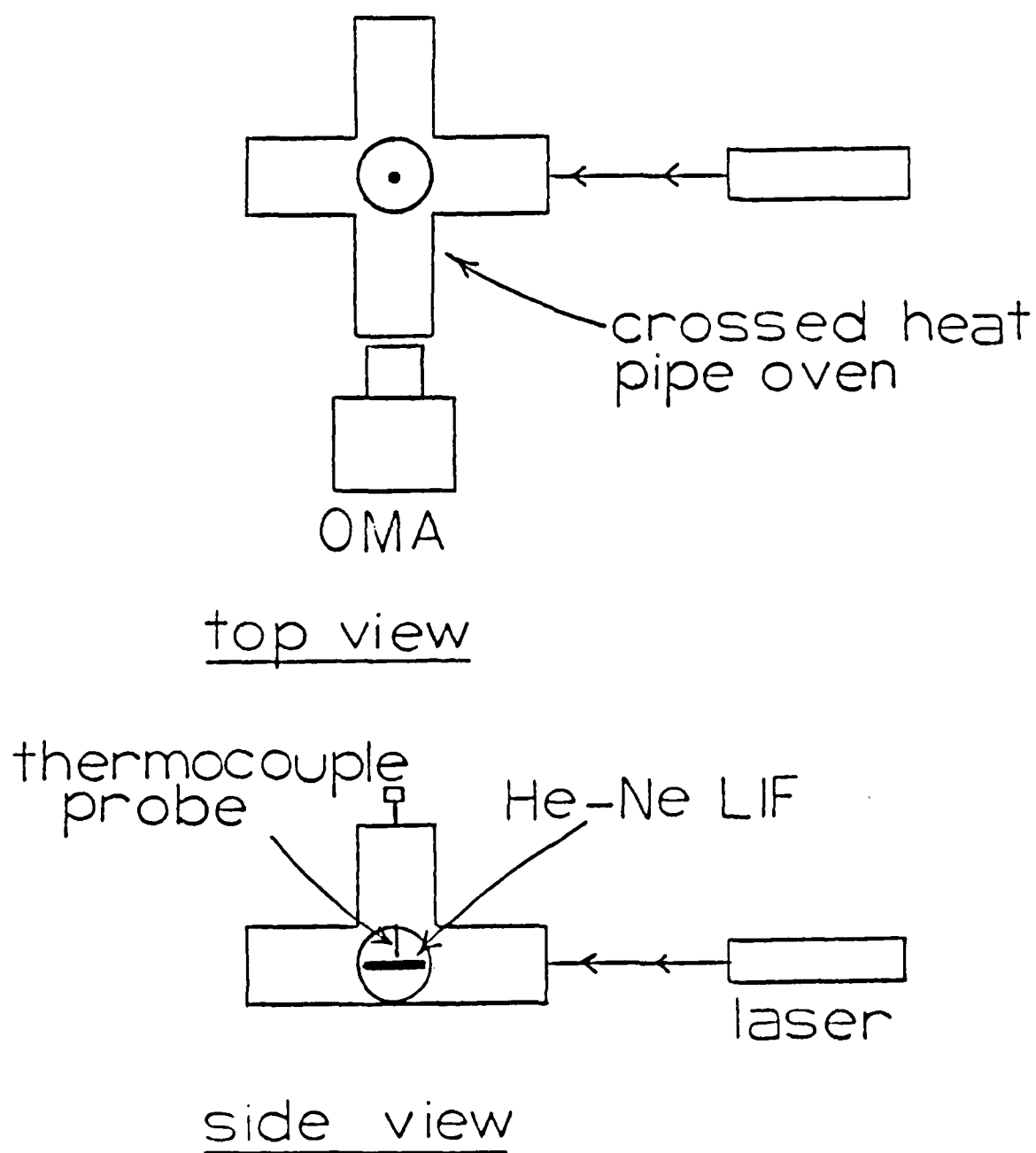


FIGURE 15 Experimental arrangement used for obtaining a temperature calibration curve.

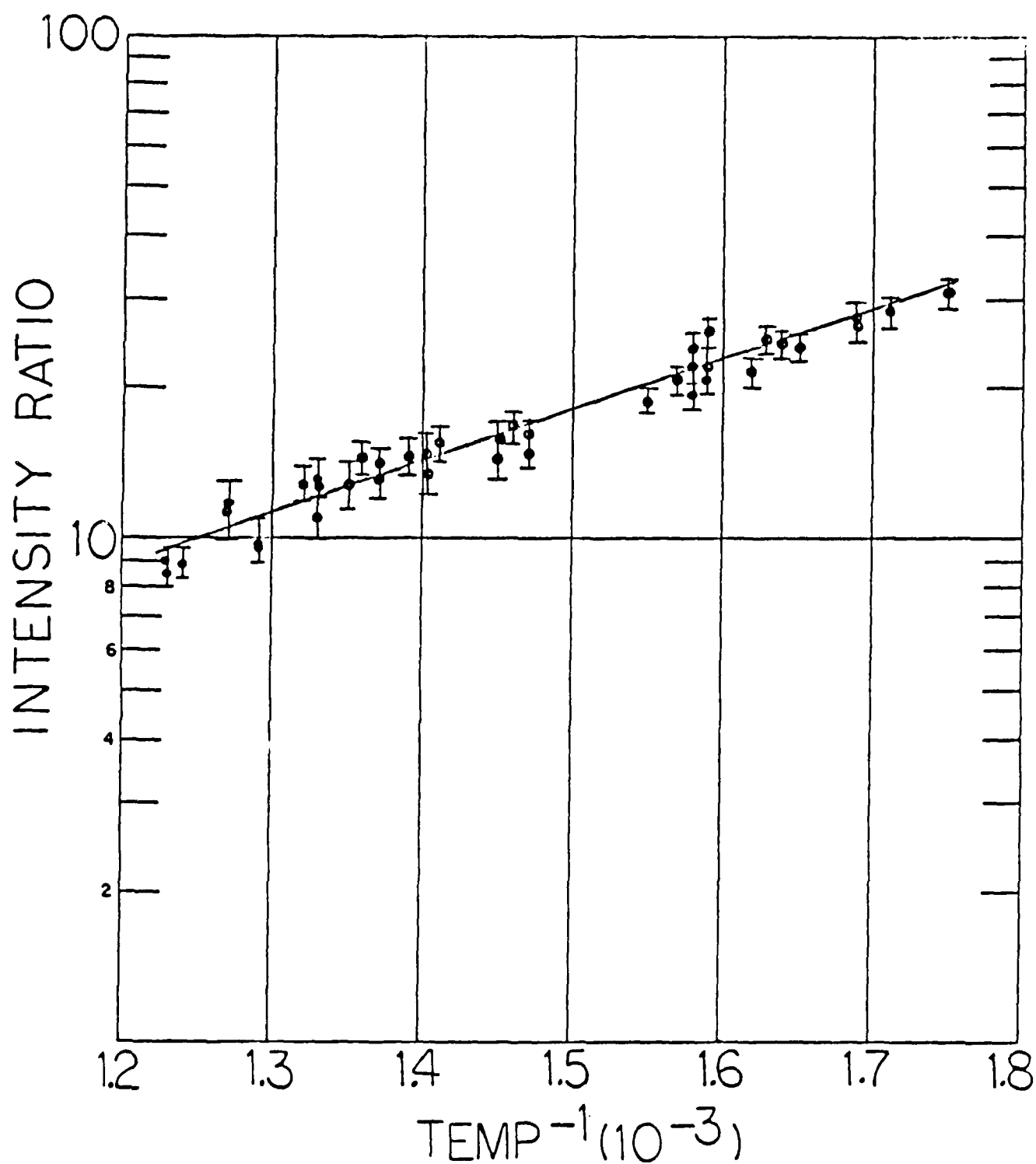


FIGURE 16 Temperature calibration curve. Y axis is the ratio of He-Ne LIF lines at 8074 Å and 7904 Å. The X axis is the inverse temperature in degrees kelvin.

The temperature calibration curve above has been used to determine the temperature profile in the heat trough device, the middle one in figure 12. This device was made out of a rectangular piece of stainless steel, the center hollowed out with ports on either end of the trough. The top is open with an O-ring seal for a glass top, allowing access for broadband optical pumping. Temperature profiles for both the axial direction and the vertical direction were made utilizing the LIF method explained above. Figure 17a is a plot of the temperature versus axial position, figure 17b the temperature versus vertical position. As these plots show, significant temperature gradients exist in the operation of this device. Various configurations of the wick were tried, with some configurations providing a more uniform vertical temperature distribution, but the axial temperature profiles did not vary much. Though the temperature profile within this device was not ideal, the top window stayed clean for long periods of time with a relatively hot (400 degrees C) sodium vapor in the device. This device deviates from the standard heat pipe oven in a number of ways, which in hindsight contribute to the poor temperature profiles measured. The geometric requirements of a long evaporation region as compared to the width of the region is obviously not satisfied, as well as the non-uniform heating provided by the flat ceramic heater placed only on the bottom. With these thoughts in mind, a new device was built which satisfies the geometric requirements for proper operation of a heat pipe, and is diagrammed in the bottom of figure 12.

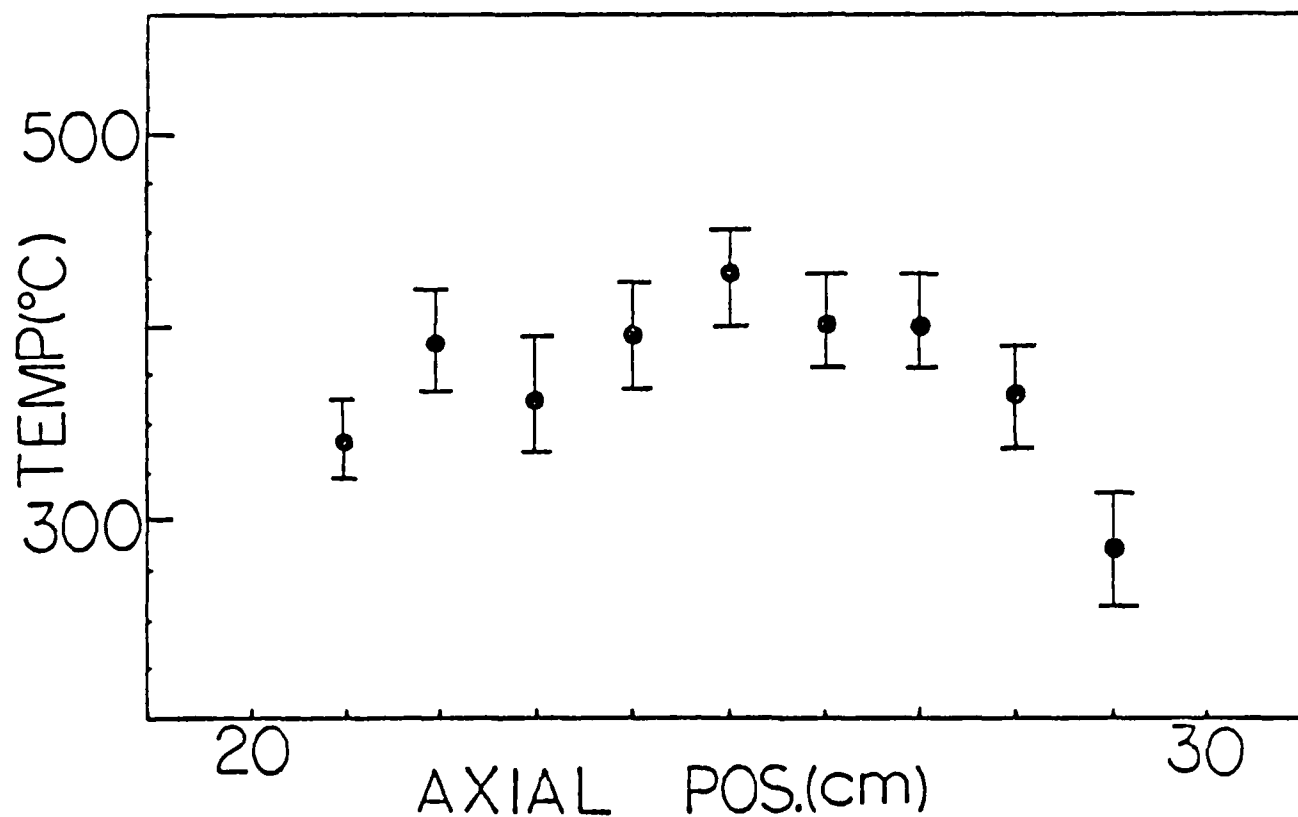


FIGURE 17a Axial temperature profile of heat trough device shown in the middle of figure 12.

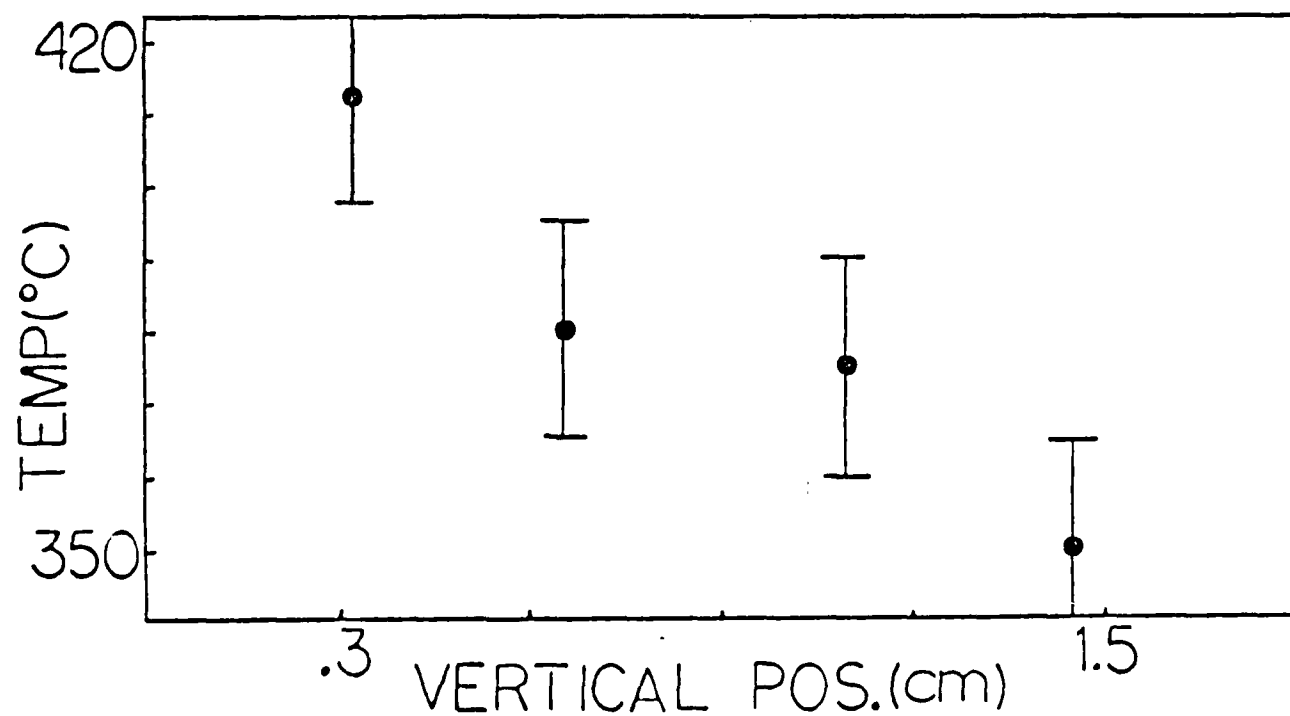


FIGURE 17b Vertical temperature profile of heat trough

The main body of this device is a one inch outside diameter stainless steel tube. A narrow slot about three eighths of an inch wide is made in the tube, about eleven inches long. A rectangular shaped four sided box whose width increases from about one half inch to two and one half inches is welded to the stainless steel tube. The wide end faces up and has a flange welded to it with an O-ring groove for sealing of the glass window. The ends are sealed with an Ultra-Torr coupling between the tube and a quartz tube with a Brewsters angle window attached. Two hemispherical cylindrical heaters are used to heat the tube in the evaporator region, which is about eleven inches long, the length of the slot in the tube. The geometry of this device conforms more to the requirements of a standard heat pipe oven while still allowing access for broadband optical pumping. A temperature profile has not been measured for this device yet, though it has operated at approximately 400 degrees C, with the top window remaining clean. As will be discussed in the following section, a dye laser optically pumped sodium A-state laser has been made with first the crossed heat pipe oven, and recently with the newest device. Thus, even without a temperature profile, the newest device has operated very well, and shows promise for operation as a pulsed laser pumped with a flashlamp.

## OPTICALLY PUMPED LASERS

The term optically pumped lasers (OPL), typically refers to a laser which is pumped by another laser. Because the pumping source is essentially monochromatic, a very narrow range of upper laser states will be populated which makes this a very efficient pumping scheme. As a first step in making a broadband optically pumped sodium A-state laser and to demonstrate adequate medium uniformity in our device, we first attempted to make an OPL using a dye laser. The dye laser used is a Molelectron model dye laser pumped with a pulsed nitrogen laser. The dye used was RB (Rhodamine B), which has a wavelength range from around 6000 Å up to 6400 Å. The experimental arrangement for making an OPL in the crossed heat pipe oven is shown in figure 18. The dye laser is steered to a focusing lens with a focal length of 46 cm, and into the heat pipe oven. The mirrors which make up the optical resonator have maximum reflection near 8000 Å, and are transparent to the visible pumping wavelength of the dye laser. The input mirror has a 5 m radius, the 5% output coupler is a flat mirror.

Alignment of the resonator is accomplished by adjusting the dye laser reflection from each of the mirrors through a small aperture placed at the output of the dye laser (there is a small amount of reflection of the dye laser by the mirror that can be viewed in a darkened room). The dye laser typically operates at about 1-10 Hz, with output pulse energy in the hundreds of microjoules and pulse widths on the order of 5-10 nanoseconds.

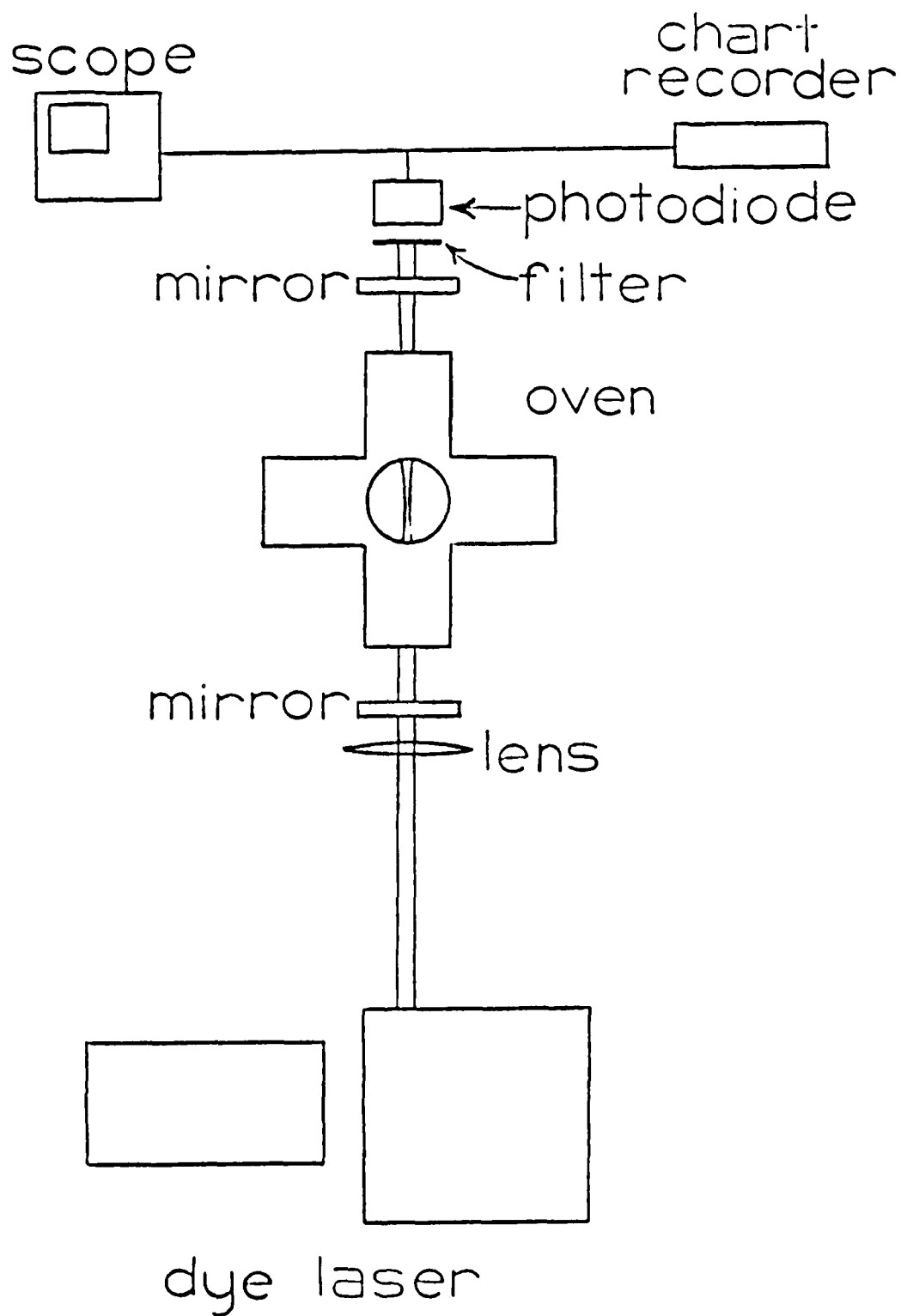


FIGURE 18 Experimental arrangement for operation of an optically pumped laser in the crossed heat pipe oven.

Lasing was achieved at a minimum temperature in the crossed heat pipe oven of around 400 °C and detected on a photodiode placed at the output coupler with its output observed on an oscilloscope. A 7800 Å cut-on filter was placed before the photodiode to stop the dye laser pulse. The dye laser was then scanned slowly from 6000 Å to 6340 Å, the photodiode output sent thru a boxcar integrater and then to a chart recorder. Hundreds of laser lines were observed as the dye laser was scanned, with a portion of the chart recording shown in figure 19. The inset of figure 19 shows an OMA spectrum for the laser line pumped at the indicated wavelength. We see that because of the bandwidth of the dye laser, a number of rotational lines are excited within some vibrational level. An assignment of the laser lines observed is beyond the scope of this program at this point, but the number of lines observed and the ease with which lasing was achieved holds promise for broadband pumping. After aligning the resonator by maximizing the photodiode output we can now replace the crossed heat pipe oven with our other devices.

I first replace the crossed heat pipe with the heat trough, without disturbing the resonator or knocking it out of alignment. The heat trough is heated up and we tried unsuccessfully to optically pump it with the dye laser. With the heat trough at its maximum temperature of around 400 °C the gain in this device is still not high enough for laser operation.

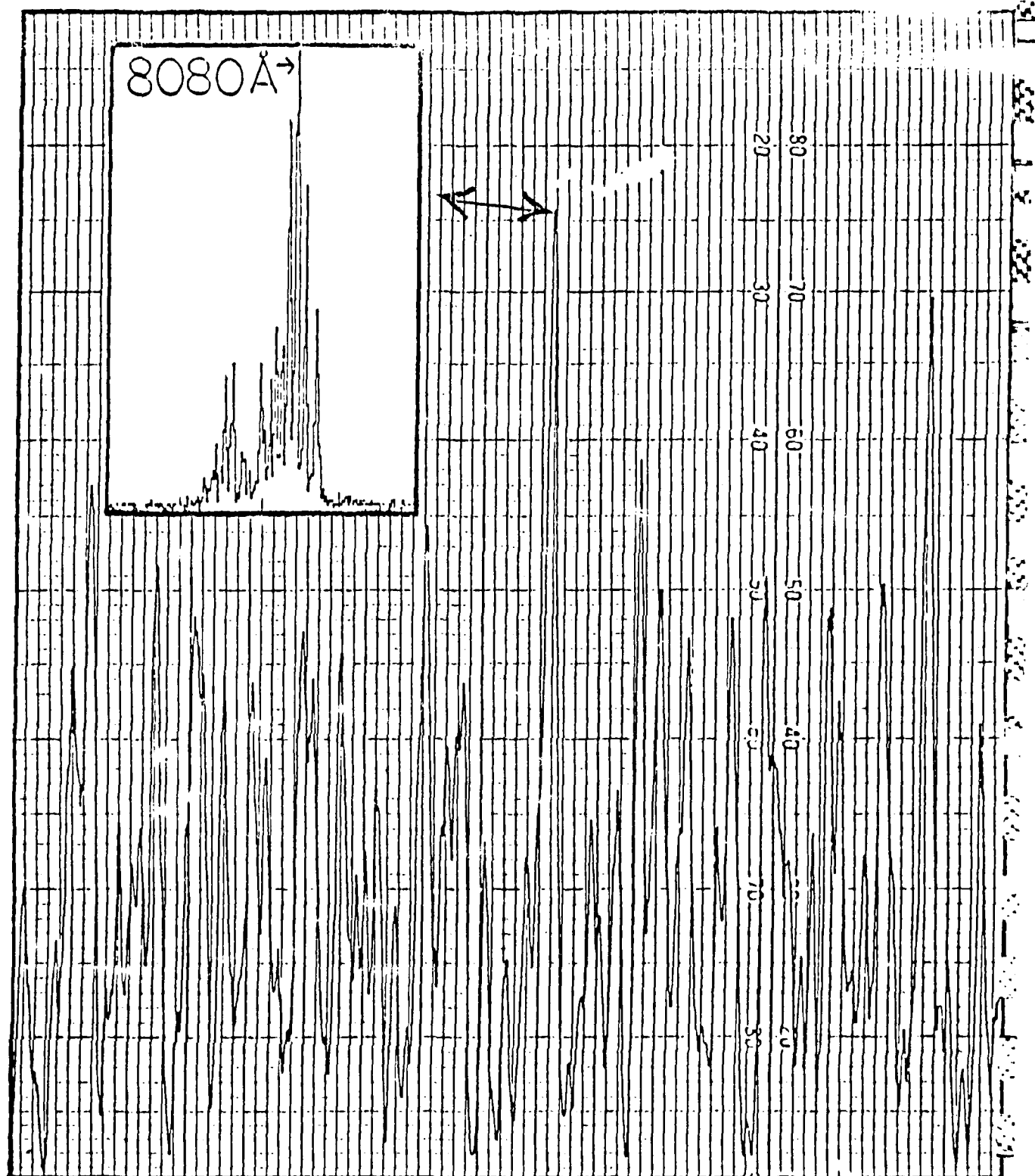


FIGURE 19 Chart recording of OPL laser output, measured with a photodiode as the pump laser is scanned. Inset is an DMA spectram of the OPL output for the indicated peak in the chart recording.

We replaced the heat trough with the latest device built, shown in the bottom of figure 12. Because of the length of this device, we had to remove the lens from its original position used for the crossed heat pipe and place it inside the resonator. This extra loss however is not a problem, since the device lases at the same tempature as the crossed-heat pipe oven, around 400 degrees C. I've operated the device for several days with only a few spots on the large window becoming discolored, and modifications of the cooling and wick configuration could possibly eliminate these small spots.

We have thus successfully made a heat pipe oven device which allows access for broadband optical pumping of the vapor zone generated inside. We have made an optically pumped sodium dimer A-state laser with the new device and observed the same spectrum of laser lines as seen in the standard crossed heat pipe oven. The operation of the device as an OPL indicates that a sufficiently uniform and dense sodium vapor can be produced and that flashlamp pumping of the device is a natural next step.

## ROTATIONAL RELAXATION

The energy levels of a diatomic molecule can be divided into three components;

- a. The electronic configuration energy (10,000's of  $\text{cm}^{-1}$  )
- b. Energy of vibration (100's of  $\text{cm}^{-1}$  )
- c. Energy of rotation (10's of  $\text{cm}^{-1}$  )

The number in parentheses after each of these refers to the approximate energy spacing between adjacent levels for each of these energies. Thus, electronic energies are several orders of magnitude larger than vibrational energies while rotational energies are an order of magnitude smaller than vibrational energies. Because the energy spacing between different rotational levels is so small, a collision between a dimer and a second body often results in a change in the rotational energy of the dimer. If the second body is an atom then it will experience a change in its kinetic energy, since the rotational energy it gains or loses is usually small compared to  $kT$ , the thermal kinetic energy. In the case of sodium vapors, the atom is the dominant vapor species and collisions between two dimers is rare so that usually dimer-dimer collisions can be ignored. In the studies we have done we have looked at the rates at which an excited electronic state of the sodium dimer has a rotation changing collision with various gases as well as with sodium atoms.

We used excited states pumped by a Helium-Neon laser for our measurements of the rate coefficient for rotation changing collisions from a particular vibration-rotation level in the  $A'\Sigma_u^+$  state of the sodium dimer. Assignment of the states pumped by the He-Ne have been documented (22), providing accurate knowledge of the parent states rotational level. The procedure we followed was to obtain spectra of the He-Ne LIF in the region of the state we chose at a variety of buffer gas pressures. The experiments were conducted in both the crossed heat pipe oven and the heat trough. The experimental arrangement for the crossed heat pipe is shown in figure 20. The He-Ne is directed down one axis of the oven, a chromel-alumel thermocouple is fed from the upper port into the vapor very close to the He-Ne path, the OMA is placed at another port while a photomultiplier tube is placed at the final port. The PMT has a 7150 Å cut-on filter in front of it to eliminate laser scatter and is used to monitor the total fluorescence induced by the laser. It is important to note that the crossed heat pipe oven is not being operated in the heat pipe mode, but is just being operated as a cell where mixing of the buffer gas and sodium vapor will occur. For each of the buffer gases studied, Xe, Ar, N<sub>2</sub>, and He, we obtain an OMA spectra for a number of different pressures. We record the temperature at each of the pressures and we record the total fluorescence associated with each of the spectram.

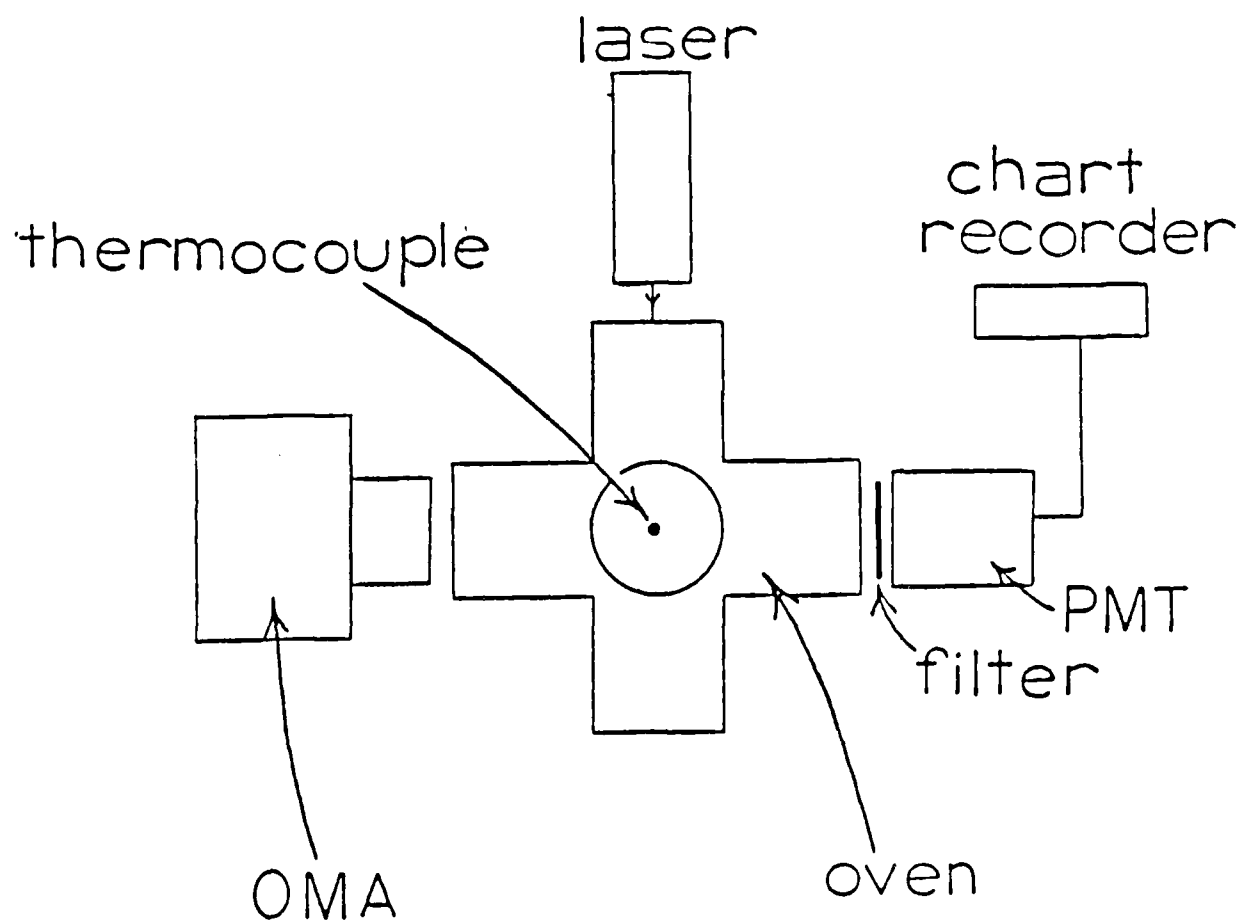


FIGURE 20 Experimental arrangement for the study of rotation changing collisions between the  $A'\Sigma_u^+$  state of  $\text{Na}_2$  and a second body.

Analysis of the data begins by considering the rate equation for the population of the state we are studying ( $\text{Na}_2(\text{A}; v'=14, J'=45)$ ),

$$1.) \quad d[\text{Na}_2(\text{A}; v'=14, J'=45)]/dt = R_{\text{pump}} - A[\text{Na}_2(\text{A}; v'=14, J'=45)] \\ - k_0[\text{Q}][\text{Na}_2(\text{A}; v'=14, J'=45)] - k_{\text{Na}}[\text{Na}][\text{Na}_2(\text{A}; v'=14, J'=45)] \\ - k_{\text{Na}_2}[\text{Na}_2][\text{Na}_2(\text{A}; v'=14, J'=45)]$$

where

$R_{\text{pump}}$  = Pumping rate

$A$  = Einstein A coefficient

$[\text{Na}_2(\text{A}; v'=14, J'=45)]$  =  $\text{Na}_2$  pressure (density) with  $v', J'$

$k_0$  = rate constant for rotation changing collisions by buffer gas

$[\text{Q}]$  = buffer gas pressure (density)

$k_{\text{Na}}$  = rate constant for rotation changing collisions by atomic Na

$[\text{Na}]$  = atomic sodium pressure (density)

$k_{\text{Na}_2}$  = rate constant for rotation changing collisions by  $\text{Na}_2$

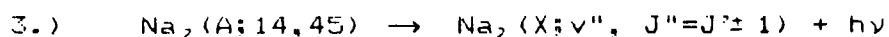
$[\text{Na}_2]$  = total sodium diatomic pressure (density)

The rate constants  $k_0$ ,  $k_{\text{Na}}$ , and  $k_{\text{Na}_2}$  are actually rate constants for the total removal of the dimer from the ( $\text{Na}_2(\text{A}; v'=14, J'=45)$ ) state which includes vibration changing collisions and electronic quenching of the molecule in which it is removed from the excited electronic state to the ground state. However, because of the large energy transfer needed for vibrational or electronic relaxation, we ignore them in these measurements and treat the rate constants as rotation changing rates. In steady state, the above time

derivative for the state  $[\text{Na}_2(\text{A}; v'=14, J'=45)]$  can be set equal to zero. We will assume the pumping rate  $R_{\text{pump}}$  is proportional to the total fluorescence and that the last term is negligible. We now have the following equation, with  $I_{\text{tot}}$  the total fluorescence as measured by the FMT, and  $[\text{Na}_2(\text{A}; 14, 45)] = [\text{Na}_2(\text{A}; v'=14, J'=45)]$  ;

$$2.) \quad I_{\text{tot}} = A[\text{Na}_2(\text{A}; 14, 45)] + k_d[Q][\text{Na}_2(\text{A}; 14, 45)] + k_{\text{na}}[\text{Na}][\text{Na}_2(\text{A}; 14, 45)]$$

The excited state  $\text{Na}_2(\text{A}; v'=14, J'=45)$  will radiatively relax to the the ground state according to the equation,



with  $v''$  = ground state vibrational level  
 $J''$  = ground state rotational level  
 $= J' \pm 1$

The selection rule  $\Delta J = \pm 1$  for homonuclear diatomic molecules results in a fluorescence spectrum which has a series of doublets closely spaced together corresponding to the two transitions of 3.) above for a given  $v''$ . There is no selection rule for the change in the vibration quantum number  $v$ , though the Franck-Condon factor will determine the relative probabilities for a transition from  $v'$  to  $v''$ . In figure 21 are two DMA spectra for the He-Ne LIF at two different pressures. Note the series of P-R doublets

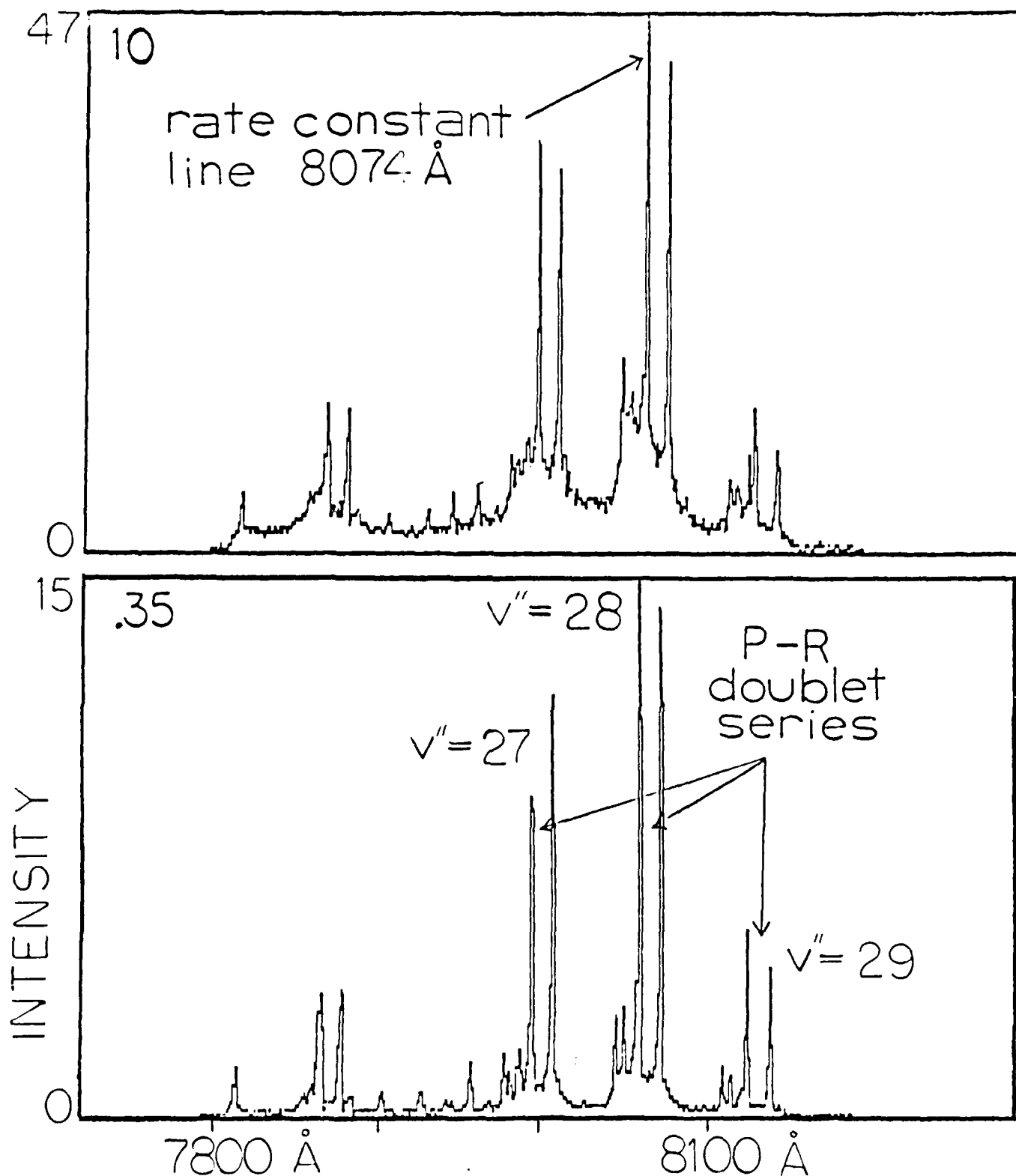
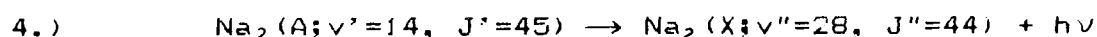


FIGURE 21 He-Ne LIF spectra of  $\text{Na}_2(\text{A})$  with Xe buffer gas at .35 and 10 Torr. Note the series of P-R doublets and the line used for determining rotation changing collision rate constants.

( F corresponds to  $J = 1$ , R corresponds to  $J = -1$  ) evident in both of the spectrum. These doublets correspond to radiative transitions from  $\text{Na}_2(\text{A}; v'=14, J'=45)$  to  $\text{Na}_2(\text{X}; v'', J'' = J' \pm 1)$ , with  $v''$  noted on the spectra. We will use the fluorescence line for the transition,



this being the strongest peak in the spectrum.

We will refer to the intensity of the fluorescence corresponding to the transition in 4.) above as  $I_{8074}$  since  $8074 \text{ \AA}$  is the wavelength of the photon emitted. The measured intensity of this line can be expressed as

$$5.) \quad I_{8074} = cA[\text{Na}_2(\text{A}; v'=14, J'=45)]$$

with  $c = \text{a constant factor.}$

Dividing equation 2.) by equation 5.) we obtain,

$$6.) \quad I_{\text{TOT}} / I_{8074} = 1/c + k_Q[\text{Q}]/cA + k_{\text{Na}}[\text{Na}]/cA$$

where the density of the  $\text{Na}_2(\text{A}; v'=14, J'=45)$  state has been factored out. We can eliminate the constant factor  $c$ , which is dependent on the experimental set up, by considering the ratio of equation 6.) for

different pressures. We experimentally determine  $I_{TOT} / I_{8074}$  at a number of pressures, and by taking the ratio of  $I_{TOT} / I_{8074}$  at one pressure to all the other pressures we get a set of pressure dependent data from which  $k_a$ , or  $k_{Na}$  can be determined. Consider 2 buffer gas pressures, P1 and P2, plugging each into 6.) above taking their ratios and rearranging, we get

$$7.) \quad ((K12 + (k_{Na}/A)(K12[Na]_1 - [Na]_1) - 1) / ([P1]/[P2] - K12)) \\ = [P2](k_a/A)$$

where  $K12 = [(I_{TOT}(P1)/I_{8074}(P1)) / (I_{TOT}(P2)/I_{8074}(P2))]$   
 Since K12 is measured, [P1] and [P2] the known buffer gas pressures,  $[Na]_1$ , the known atomic sodium pressure at the two buffer gas pressures and  $k_{Na}$  a measureable quantity, we can use 7.) to determine  $k_a$ , as follows. By keeping [P1] in 7.) above constant and varying [P2], a plot of the left hand side of equation 7.) versus [P2], will have a slope which is proportional to  $k_a$ , for sufficiently low pressures where multiple collisions can be ignored. As is clear in figure 21, the intensity  $I_{8074}$  decreases as the buffer gas pressure increases, since the number of rotation changing collisions increases. Also note the increase in the background in the region of the 8074 line, due to the radiation from those states which become populated from the parent state  $Na_2(A; v'=14, J'=45)$  by these rotation changing collisions. The intensity  $I_{8074}$  is

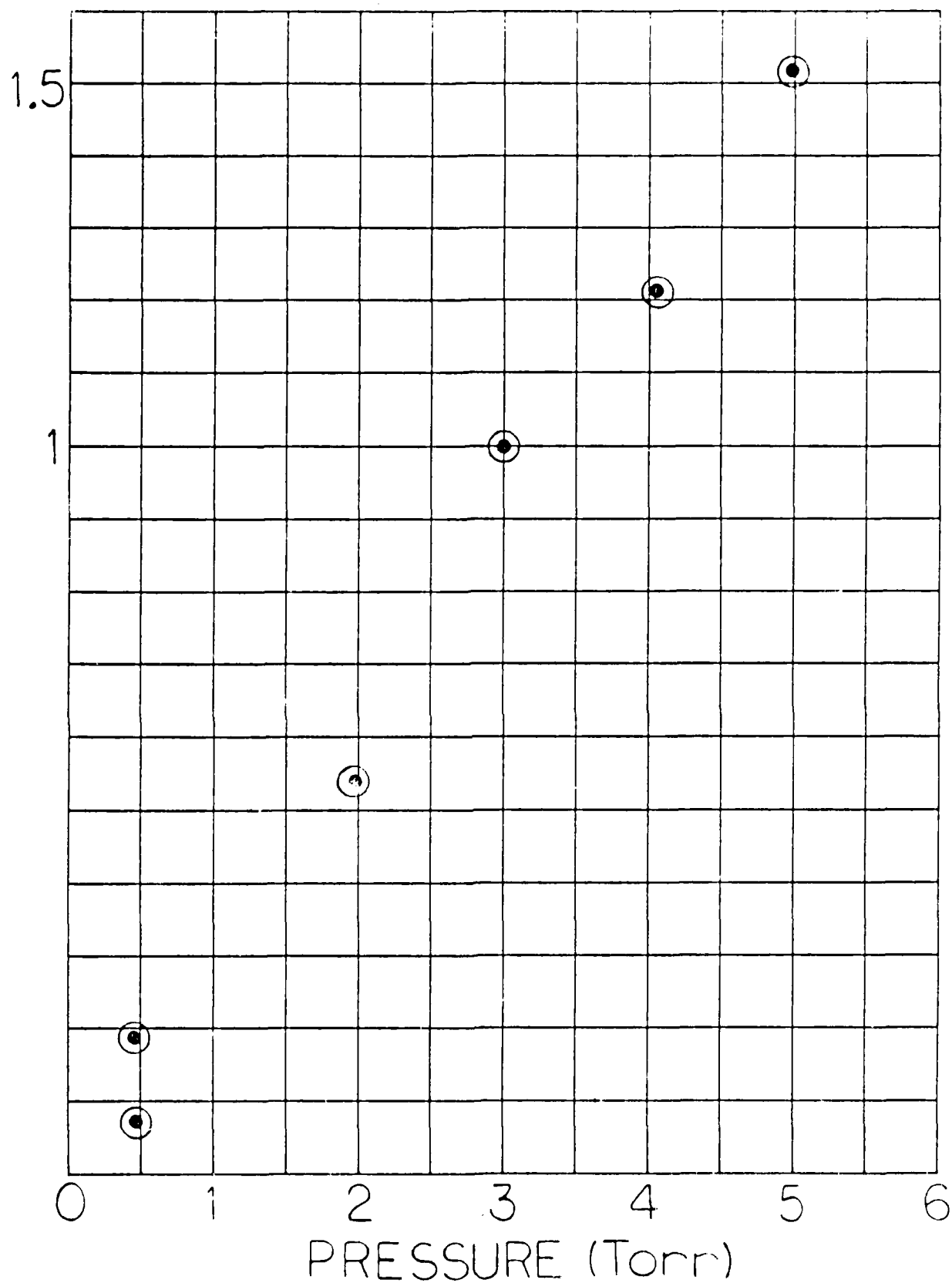


FIGURE 22 Plot of left side of equation 7.) versus Helium pressure. Slope is rate constant times the radiative lifetime of  $\text{Na}_2(A, 14, 45)$ .

measured from the top of this background, since some of this peak and background could be due to states which have been collisionally populated from parent states other than the 8074 state. A plot of the left side of equation 7.) versus  $[P_2]$  for the case of Helium as the buffer gas is shown in figure 22. The rate constant is determined by multiplying the slope by A.

We determine  $k_{Na}$ , the rate constant for rotation changing collisions between the sodium dimer and the atom in a similar manner. These measurements are made in the heat pipe oven with it operating in the heat pipe mode, since under these conditions only sodium vapor exists in the evaporator region where the measurement are being made. In this case the buffer gas pressure is zero in the region of observation, and equation 7.) becomes

$$8.) \quad \left\{ (1 - k_{12}) / (k_{12} - [Na]_1 / [Na]_2) \right\} = [Na]_2 (k_{Na} / A)$$

with  $[Na]_1$  = standard sodium pressure

$[Na]_2$  = variable sodium pressure

A plot of the left hand side of 8.) versus  $[Na]_2$  will have a slope which is proportional to  $k_{Na}$ , again the proportionality constant being  $1/A$ . We now use this rate constant for sodium,  $k_{Na}$ , in equation 7.) to obtain the rate constant  $k_2$ , for the gases Xe, Ar,  $N_2$ , and He used in these studies.

The table below summarizes the preliminary results obtained so far for the rate constants for rotation changing collisions between  $\text{Na}_2$  (A:14.45) and a second body.

GAS	PRESSURE RANGE	TEMPATURE RANGE	RATE CONSTANT (10 <sup>-10</sup> NS TORR <sup>-1</sup> )
Na	.28 - 2 Torr	390 - 540 C	2.5
Xe	.35 - 2 Torr	409 - 345 C	2.2
Ar	.20 - 5 Torr	367 - 331 C	2.3
N	.20 - 5 Torr	380 - 348 C	4.1
He	.20 - 3 Torr	390 - 378 C	4.6

## CONCLUDING REMARKS

Efforts to develop a broadband optically pumped sodium dimer laser have been reviewed. The concept for pooling of solar radiation energy into the narrow atomic D-line radiation and absorption of this energy to the upper laser state was introduced. Up to 20% of the solar radiation could be absorbed via this mechanism, which combined with the high gain medium of a hot (900 K) sodium vapor provide the means for making a directly solar pumped laser. Development of a heat pipe oven device which has access for broadband pumping while maintaining a hot sodium vapor is well under way. One such device has been operated as an OPL, with vapor temperatures in the 400-500 C range and the large window remaining relatively clean. Flashlamp pumping of the sodium vapor is the next step in the experimental program.

A method for measuring temperature profiles using He-Ne LIF was introduced and the temperature profile of one heat pipe oven device presented. This method uses the Boltzmann distribution among the ground state vibrational levels as the basis for measuring the temperature. Rate constants for rotation changing collisions between an excited state of the sodium dimer and various gases were measured. Our preliminary results are smaller than values found in the literature(22), though the state we studied was different from the states studied in Ref. (22) and might affect the value.

## REFERENCES

- (1) Rather, J. D. G., "New Candidate Lasers for Power Beaming and Discussion of Their Applications," in Radiation Energy Conversion in Space, ed. by K. W. Billman, Vol. 61, p. 313 of Progress in Astronautics and Aeronautics (1978).
- (2) Monson, D. J., "Systems Efficiency and Specific Mass Estimates for Direct and Indirect Solar-Pumped Closed-Cycle High-Energy Lasers in Space," *ibid.* p. 333.
- (3) Ham, David O. "Solar Pumped, Alkali Vapor Laser," Final Report Physical Sciences Inc. Research Park, Andover, MA 01810.
- (4) Wellegehausen, B., "Optically Pumped Alkali Molecule Lasers," in "Metal Bonding and Interactions in High Temperature Systems with Emphasis on Alkali Metals," J. L. Gole and W. C. Stwalley, eds., ACS Symp. Ser. 179, p 461 (1982).
- (5) Callender, R. H., Gersten, J. I., Leigh, R. W. and Yang, J. L., "Dependence of Transition Moment on Internuclear Separation in Na<sub>2</sub>," *Phys. Rev. Lett.* 32, 917 (1974).
- (6) Callender, R. H., Gersten, J. I., Leigh, R. W. and Yang, J. L., "Role of Metastable Dimers in the Theory of Induced Atomic Fluorescence," *Phys. Rev. Lett.* 33, 1311 (1974).
- (7) Kraulinaya, E. K. and Yanson, M. L., "Atomic Excitation Processes During the Absorption of Laser Radiation by Alkali-Metal Molecules," *Opt. Spectrosc. (USSR)* 46 629 (1979).
- (8) Valley, S. L., ed., "Handbook of Geophysics and Space Environments," Section 16.1 by P. R. Gast on "Solar Electromagnetic Radiation," McGraw-Hill Book Co., Inc. (1965).
- (9) Kibble, B. P., Copley, G. and Krause, L., "Effect of Imprisonment of Radiation in Sodium Vapor on the Measured Lifetime of the 3 P States," *Phys. Rev.* 153, 9 (1967).
- (10) Garver, W. P., Pierce, M. R. and Leventhal, J. J., "Measurement of Atomic Densities Using Radiation Trapping," *J. Chem. Phys.* 77, 1201 (1982).
- (11) Huennekens, J. and Gallagher, A., "Radiation Diffusion and Saturation in Optically Thick Na Vapor," *Phys. Rev. A* 28, 238 (1983).
- (12) Holstein, T., "Imprisonment of Resonance Radiation in Gases I," *Phys. Rev.* 72, 1212 (1947), and II, *Phys. Rev.* 83, 1159 (1951).

- (13) Milne, E., J. London Math. Soc. 1, 1 (1926); presented in A. C. G. Mitchell and M. W. Zemansky, "Resonance Radiation and Excited Atoms," p. 196, Cambridge University Press (1961).
- (14) Henesian, M. A., Herbst, R. L., and Byer, R. L., "Optically Pumped Superfluorescent Na<sub>2</sub> Molecular Laser," J. Appl. Phys., 47, 1515 (1976).
- (15) Bahns, J. T., Rajaei-Rizi, A. R., Verma, K. K., Orth, F. B. and Stwalley, W. C., "New Alkali Metal Dimer Optically Pumped Lasers," Proc. Int. Conf. on Lasers '82, 713 (1983).
- (16) Itoh, J., Uchiki, H. and Matsuoka, M., "Stimulated Emission from Molecular Sodium," Opt. Commun. 18, 271 (1976).
- (17) D. O. Ham, unpublished results
- (18) Grover, G. M., Cotter, T. P. and Erickson, G. F., "Structures of Very High Thermal Conductance," J. Appl. Phys. 35, 1990 (1964).
- (19) Vidal, C. R. and Cooper, J., "Heat-Pipe Oven: A New, Well-Defined Metal Vapor Device for Spectroscopic Measurements," J. Appl. Phys. vol. 40, 8, (1969).
- (20) Rohani, A. R. and Tien, C. L., "Minimum Heat Transfer Limit in Simple and Gas Loaded Heat Pipes," AIAA Journal, vol. 13 no. 4 (1974).
- (21) K. K. Verma, T. H. Vu, and W. C. Stwalley, "New Observations and Analyses of the Laser Excited Fluorescence of the A'<sup>2</sup>Σ<sub>g</sub><sup>+</sup>-X'<sup>2</sup>Σ<sub>g</sub><sup>+</sup> Bands of the Na<sub>2</sub> Molecule," J. Molec. Spectrosc. 85, p. 131 (1981)
- (22) Timothy A. Brunner, Neil Smith, Allan W. Karp, and David E. Pritchard, "Rotational Energy Transfer in Na<sub>2</sub><sup>+</sup>(A) colliding with Xe, Kr, Ar, Ne, H<sub>2</sub>, CH<sub>4</sub>, and N<sub>2</sub>: Experiment and Fitting Laws," J. Chem. Phys., Vol. 74, No. 6, 15 March 1981.

END

JAN.

1988

DTIC